

**Improved Performance
of a Virtually Imaged Phased Array
for Optical Demultiplexing**

by

Afsana N. Akhter

Submitted to the Department of Electrical Engineering and Computer
Science in partial fulfillment of the requirements for the degree of

Master of Engineering

at the

MASSACHUSETTS INSTITUTE OF TECHNOLOGY

May 19, 1999

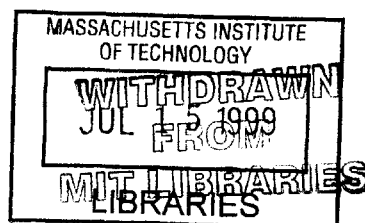
June 1999

© Massachusetts Institute of Technology, 1999. All Rights Reserved.

Author
Department of Electrical Engineering and Computer Science
May 19, 1999

Certified by
Hermann A. Haus
Institute Professor
Thesis Supervisor

Accepted by
Arthur C. Smith
Chairman, Department Committee on Graduate Students



ENG

Improved Performance of a Virtually Imaged Phased Array for Optical Demultiplexing

by

Afsana N. Akhter

Submitted to the Department of Electrical Engineering
and Computer Science on May 20, 1998 in fulfillment of
the requirements for the degree of

Master of Engineering in Electrical Engineering

Abstract

In fiber optic communication, the transmission of multiple optical channels over the same fiber provides a simple way for making use of the unprecedented capacity offered by optics. Optical demultiplexing is a critical function in high density wavelength division multiplexing for channel spacing of 1 nanometer or less. A Virtually Imaged Phased Array (VIPA) produces a large angular dispersion that can be applied to optical demultiplexing. A mathematical model of the VIPA system is developed. Using this model, a numerical simulation of the VIPA demultiplexer is constructed and then used to develop VIPA designs with improved performance. Results show that a glass plate with linear transmissivity increases VIPA's efficiency and reduces channel crosstalk. The simulation was also used to perform a perturbation analysis of the system. If the plate in the VIPA is of non-uniform thickness, considerable beam distortion occurs, which increases channel crosstalk. It is demonstrated that the distortion due to a linearly varying plate thickness can be corrected using a proper lens system.

Thesis Advisor: Hermann A. Haus

Title: Institute Professor

Acknowledgments

I would like to thank Dr. Masataka Shirasaki for his guidance and support. He is a great teacher whose knowledge and patience never ceased to amaze me. I have learned a great deal from him.

I am honored to have had Professor Hermann A. Haus as my advisor and am grateful to him for the opportunity to take part in this project. His guidance and encouragement has made this an extremely rewarding experience for me.

I thank Christopher Lin for being a great partner in this project and wish him good luck as he continues work with the VIPA system. I thank my office-mates Charles Yu and Pat Chou and my other friends in the group for their great company.

I am forever grateful to my high school teachers and mentors: Mr. Shaukat, Mr. Majid, Mr. Fakuiddin, and Dr. Haq, who continue to inspire me. Finally, I thank my family and friends who make the endless toil bearable and the rest so enjoyable.

Contents

1.0 Introduction	9
1.1 Scope of thesis.....	10
1.2 Simulation Code and facilities.....	11
2.0 Background	12
2.1 Fiber Optic Communication Systems.....	12
2.2 WDM Systems, Multiplexers, and Demultiplexers.....	13
2.3 Single Mode Fibers.....	14
2.4 The Gaussian Beams.....	15
2.5 The Lorentzian Beam.....	15
2.6 Optical Fourier Transform.....	16
2.7 Propagation Through Free Space: Fresnel Diffraction.....	17
2.8 Propagation through a lens.....	18
3.0 VIPA Demultiplexing Method (<i>page 12</i>).....	20
3.1 Optical Demultiplexing using VIPA.....	20
3.2 Angular Dispersion.....	22
3.3 Polarization Dependence.....	22
3.4 Comparison of VIPA with other Demultiplexers.....	23
4.0 VIPA Simulation Model	24
4.1 Computing VIPA Field Distributions.....	24
4.2 Power loss at Window of glass plate.....	29
4.3 Optimal Beam Waist Size, Window Size, and IncidentAngle.....	31
4.4 Overall Efficiency of VIPA system.....	33

4.4.1 Power Loss at Window.....	33
4.4.2 Power Loss to Sidelobes.....	34
4.4.3 Coupling Efficiency.....	35
4.5 Multiwavelength Input.....	37
5.0 Simulation Results	38
5.1 VIPA with Uniform Transmissivity.....	38
5.1.1 Field Profiles Inside Glass Plate.....	38
5.1.2 Output Field Profiles.....	40
5.1.3 Efficiency of VIPA with Uniform Transmissivity.....	43
5.2 VIPA with Linearly Varying Transmissivity.....	45
5.2.1 Output Field Profiles	45
5.2.2 Efficiency of VIPA with Linearly Varying Transmissivity.....	47
5.3 Far Field Output for Multi-wavelength Input.....	48
5.4 Effects of Varying Plate Thickness.....	49
5.5 Angular Dispersion.....	53
5.6 Cross-talk from Neighboring Channels.....	54
6.0 VIPA with non-parallel glass plate.....	57
6.1 VIPA model using plate with linearly varying thickness.....	57
6.2 Beam Distortion produced by non-uniform plate.....	58
6.3 Method of correcting beam distortion.....	61
7.0 Summary and Conclusion	65
8.0 Bibliography.....	66
9.0 Appendix: Simulation Code.....	67

List of Figures

Figure 2-2-1:	Wavelength Division Multiplexing	13
Figure 2-3-1:	Single mode fibers.	14
Figure 2-5-1:	Lorentzian function.	16
Figure 2-8-1:	Propagation of a beam through a lens.	19
Figure 3-1-1:	Schematic of a VIPA demultiplexing system.	20
Figure 3-1-2:	Detailed VIPA structure showing virtual images.	21
Figure 4-1-1:	Base coordinate system of VIPA model along with glass plate.	24
Figure 4-1-2:	Beam positions inside the glass plate after successive reflections.	26
Figure 4-2-1:	Illustration of Power loss at window of glass plate.	30
Figure 4-3-1:	Graph of beam width at window versus beam waist at point of incidence.	32
Figure 5-1:	Magnitude and phase profiles of beam inside the plate.	39
Figure 5-2:	Magnitude and phase of total transmitted field just outside the plate.	41
Figure 5-3:	Magnitude profile of focused output using uniform transmissivity.	41
Figure 5-4:	Lorentzian mainlobe of focused output and its inverse Fourier transform.	42
Figure 5-2-1:	Linear transmission amplitude and corresponding reflection profile.	45
Figure 5-2-1-1:	Far field output pattern using linear transmissivity.	45
Figure 5-2-1-2:	Symmetric mainlobe of farfield output and its inverse Fourier Transform.	46
Figure 5-3-1:	Demultiplexed output of ten channels for two different incident angles.	48
Figure 5-4-1:	Demultiplexed output of ten channels for different plate thicknesses.	50
Figure 5-4-2:	Adjusting plate thickness to keep 1550nm mainlobe at envelope peak.	52
Figure 5-5-1:	Plot of output angle as a function of wavelength	54

Figure 5-6-1:	Crosstalk characteristic of uniform transmissivity and linear transmissiity.	55
Figure 6-1-1:	Model of VIPA glass plate with linearly varying plate thickness	58
Figure 6-1-2:	Linear amplitude transmissivity and corresponding reflectivity profiles . .	58
Figure 6-2-1:	Comparison of output of plate of linear thickness with ideal case	59
Figure 6-2-2:	Comparison of near field output magnitude and phase profiles of plate of linear thickness with the ideal case.60
Figure 6-2-3:	Quadratic phase distortion produced by plate with nearly varying thickness for different wavelengths60
Figure 6-3-1:	Comparison of demultiplexed output of ideal case and output of linear thickness plate compensated by a cylindrical lens62
Figure 6-3-2:	Quadratic phase minus parabolic phase of cylindrical lens for different wavelengths62
Figure 6-3-3	Output of plate with linear thickness using cylindrical lens and output fibers arranged on tilted plane campared with ideal output.63
Figure 6-4-1	Comparison of VIPA systems using parallel glass plate; correcting cylindrical lens only; cylindrical lens and output fibers on tilted plane64

List of Tables

Table 3-4	Comparison of VIPA to other demultiplexers.23
Table 4-1	Expressions for reflection and transmission profiles.	25
Table 5-4	Parameters of different incident angles and plate thicknesses.	53

Chapter 1 Introduction

With the advent of the ‘information superhighway’ and the explosive growth of the graphics driven World Wide Web, the demand for high bit rate communication systems has been rising exponentially. The signal bandwidth in optical communication systems can exceed 1 THz due to a large carrier frequency associated with the optical carrier. The transmission of multiple optical channels over the same fiber provides a simple way for making use of the unprecedented capacity offered by optics. To optimize the use of bandwidth, it is desirable to send as many channels as possible over the same fiber. The reduced spacing between channels requires highly sophisticated methods to ensure the integrity of the information transmitted through the channels [5].

Optical multiplexing /demultiplexing is a critical function in high density wavelength division multiplexing systems for channel spacing of the order of 1 nanometer or less. Multiplexers combine the output of several transmitters and launch it into an optical fiber, while demultiplexers split the received multichannel signal into individual channels destined to different receivers.

Existing demultiplexing technologies for such multi-channel systems, such as Fabry-Perot or Mach-Zehnder interferometers, require that a number of these splitters be cascaded. While diffraction gratings provide a much simpler means of decomposing light into many wavelengths at a time, they bear certain disadvantages. Their diffraction efficiency depends on the polarization-state and they exhibit insufficient angular dispersion. Because of this low dispersion, the multi-

plexer/demultiplexer for dense channels is not compact and its characteristics are sensitive to misalignment [1].

The virtually imaged phased array (VIPA) is a new optical technique that produces a large angular dispersion. This novel method was developed by Dr. Masataka Shirasaki at Fujitsu Labs, Japan, in 1995 [1]. The angular dispersion of a VIPA is about 10-20 times larger than those of common diffraction gratings which have blaze angles of about 30 degrees. With the current configuration of the VIPA, wavelength demultiplexing for 10 channels with 0.8 nm spacing is achieved. Its other advantages are that it has a very low dependence on input polarization state and its structure is simple, compact and low cost. Table 3-4 of chapter 3 compares the VIPA demultiplexer to other demultiplexing techniques with respect to angular dispersion, polarization dependence, compactness, etc.

1.1 Scope of Thesis

This thesis describes the use of a virtually imaged phased array to achieve improved demultiplexing in DWDM systems. A numerical simulation has been constructed to analyze the performance of different VIPA demultiplexer designs and to optimize the system for maximum angular dispersion and minimum power loss. Chapter one describes the origin of the VIPA technique and its role in WDM communication systems. Chapter two provides an overview of WDM optical communication systems and briefly revises some theoretical concepts relevant to understanding VIPA. A detailed description of the basic VIPA demultiplexing technique is contained in chapter three. Chapter four describes the mathematical model of the VIPA system that is used to implement the numerical simulation. A detailed discussion of the simulation results of the different VIPA

designs appears in Chapter 5. This chapter illustrates how varying VIPA parameters affects the demultiplexers performance and how these parameters are optimized to maximize angular dispersion and minimize power loss. Chapter six contains a perturbation analysis and shows that the distortion produced by using a glass plate with linearly varying thickness can be corrected by simple optical techniques.

1.2 Simulation Code and Facilities

The simulation of the VIPA demultiplexer was implemented in Matlab version 5.2 on Sun Ultra5 and Ultra10 workstations in the Athena computing environment of M.I.T. A listing of the matlab code used to simulate VIPA appears in the appendix.

Chapter 2 Background

This chapter begins with an overview of WDM optical communication systems. It then discusses some concepts in optics and signal processing that are relevant to understanding how the VIPA technique works and how the simulation is implemented.

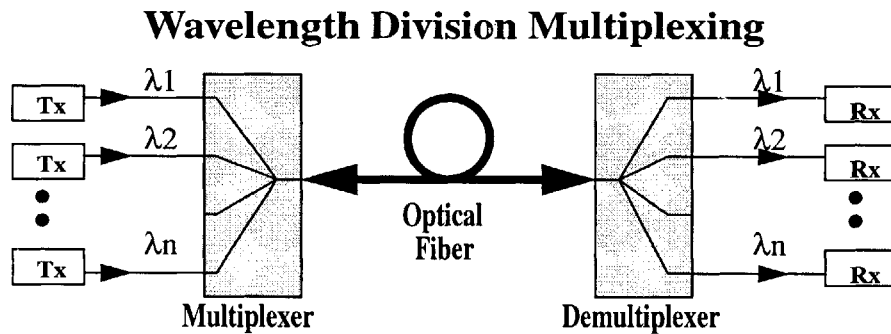
2.1 Fiber Optic Communication Systems

Transmission of data has been revolutionized by the use of the optical fiber. Optical fiber provides low loss (.25 dB/km at a wavelength of 1550nm) and high bandwidth that exceeds 1 THz, making it an ideal medium for transmitting large amounts of data over long distances. However, even though the bit rate can exceed 1 Tb/s in principle, in practice, it is often limited to 10Gb/s or less because of fiber dispersion or electronic speed limitations [5].

The attenuation coefficient and the dispersion coefficient of different types of fused-silica-glass fibers are dependent on wavelength. Minimum attenuation occurs at $\sim 1.55\mu\text{m}$, whereas the minimum material dispersion occurs at $\sim 1.312\mu\text{m}$. The choice between these two wavelengths depends on the relative importance of power loss versus pulse spreading and on the availability of an appropriate light source. Most advanced systems operate at wavelengths centered at $1.3\mu\text{m}$ and $1.55\mu\text{m}$ [5].

2.2 WDM Systems, Multiplexers and Demultiplexers

The use of multiple channels over the same fiber provides a simple way to make use of the unprecedented capacity offered by optics. Each channel is transmitted by modulating its own carrier. The carrier frequencies are separated enough that the optical spectra of the modulated channels do not overlap in frequency. The multiple channels are demultiplexed at the receiver by using frequency selective components. Lightwave systems that make use of such a scheme are known as multichannel communication systems. WDM has the potential for exploiting the large bandwidth offered by the optical fiber, as hundreds and even thousands of channels can be transmitted if the channel spacing is reduced to a few GHz by using coherent techniques[5].



The role of WDM in such systems is simply to increase the total bit rate. Figure 2-2-1 represents the scheme of a high capacity WDM system. The output of several transmitters, each operating at its own carrier frequency (or wavelength) are multiplexed together. The multiplexed signal is launched into the optical fiber for transmission to the other end, where a demultiplexer routes each channel to its own receiver. When N channels at bit rates B_1, B_2, \dots, B_n are transmitted simultaneously over a fiber of length L, the total bit rate-distance product BL becomes :

$BL = (B_1+B_2+ \dots +B_n)*L$. For equal bit rates, system capacity is enhanced by a factor of N [5].

2.3 Single Mode Fibers

The input to the VIPA demultiplexer is the multi-channel output from a single -mode fiber. An optical fiber consists of a high refractive index core surrounded by a layer of lower index cladding, as shown in figure 2-3-1. In the figure, n_1 is the refractive index of the core, n_2 is the refractive index of the cladding, and n_0 is the refractive index of air. The core and cladding diameters are given by a and b respectively. For a single mode fiber, a is in the range of 2-4 μm . Typical values for b are 50-60 μm .

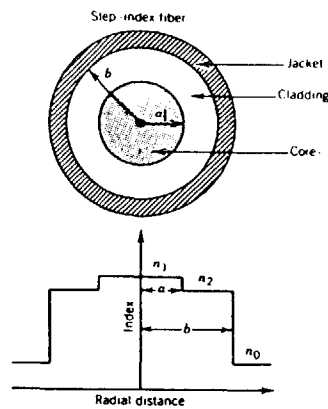


Figure 2-3-1 Single mode fiber with core of refractive index n_1 and cladding of refractive index n_2 .

Single mode fibers support only the HE_{11} mode which is also known as the fundamental mode of the fiber. The fiber is designed in such a way that all higher order modes are below cutoff at the operating wavelength. The V parameter determines the number of modes supported by a fiber as well as the cutoff condition of various modes. The fundamental mode has no cutoff and is always supported by a fiber. In practice the fundamental mode of a single-mode optical fiber is often approximated by a gaussian distribution which is described in section 2.4 [5] .

2.4 The Gaussian Beam

The gaussian beam is an important solution of the paraxial helmholtz equation that exhibits the characteristics of an optical beam. Eqn 2.4.1 gives an expression for the complex amplitude, $U(r)$, of a gaussian beam. The parameter z_0 is known as the Rayleigh range such that $W(z_0) = \sqrt{2} \cdot W_0$ and the intensity at z_0 is half the peak intensity. $W(z)$ and $R(z)$ are measures of the beam width and wavefront radius of curvature, respectively, and are expressed in terms of z and z_0 according to equations 2.4.2 - 2.4.4 [3].

$W(z)$ has a minimum value, W_0 , at the beam waist and grows gradually in both directions. The wavefronts are approximately planar near the beam waist, but they gradually curve and become approximately spherical far from the waist.

2.5 The Lorentzian Beam

$$U(r) = A_0 \frac{W_0}{W(z)} \exp\left[-\frac{\rho^2}{W^2(z)}\right] \exp\left[-jkz - jk\frac{\rho^2}{2R(z)} + j\xi(z)\right] \quad 2.4.1$$

$$W(z) = W_0 \left[1 + \left(\frac{z}{z_0}\right)^2\right]^{1/2} \quad 2.4.2$$

$$R(z) = z \left[1 + \left(\frac{z_0}{z}\right)^2\right] \quad 2.4.3$$

$$W_0 = \left(\frac{\lambda z_0}{\pi}\right)^{1/2} \quad 2.4.4$$

$$\xi(z) = \text{atan}\left(\frac{z}{z_0}\right) \quad 2.4.5$$

2.5 The Lorentzian Beam

Let $e(t)$ be an exponentially decaying harmonic function of time $e(t) = e^{-t/2\tau} e^{j2\pi\nu_0 t}$, which has an energy that decays as $e^{-t/\tau}$ (with time constant τ). The Fourier transform of $e(t)$, given by equation 2.5.2, is proportional to $1/[1 + j4\pi(\nu - \nu_0)\tau]$ and is a Lorentzian function. The Lorentzian profile, $g(\nu)$ is a function of frequency, ν , and is given by equation 2.5.1. The full width at half maximum (FWHM) of this Lorentzian function of frequency is $\Delta\nu = 1/2\pi\tau$. The value of the-

Lorentzian function at the central frequency ν_0 is given by $g(\nu_0) = 2/\pi\Delta\nu$. Figure 2-5-1 shows the symmetric magnitude and asymmetric phase profile of the Lorentzian function [3].

$$g(\nu) = \frac{(\Delta\nu)/(2\pi)}{(\nu - \nu_0)^2 + (\Delta\nu/2)^2} \quad 2.5.1$$

$$g(\nu) = \int_{-\infty}^{\infty} e(t) \cdot e^{-j\omega t} dt \quad 2.5.2$$

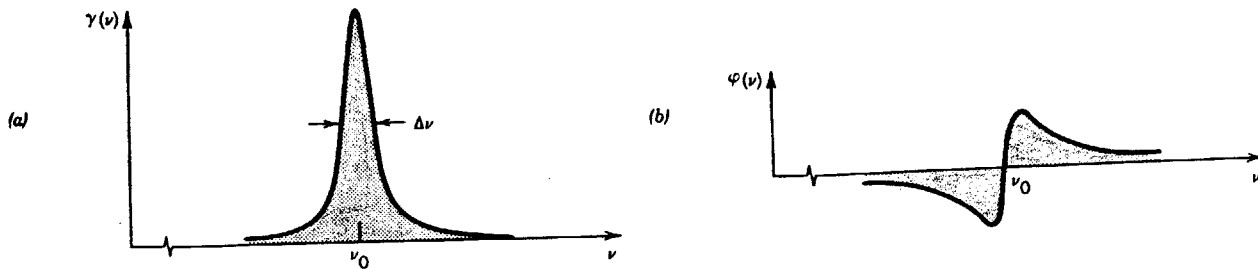


Figure 2-5-1 Symmetric magnitude and asymmetric phase profile of a Lorentzian function

2.6 Optical Fourier Transform

If $f(x,y)$ is a function of two variables and x and y represent the coordinates of a point in a two-dimensional space, then $f(x,y)$ represents the optical field in a given plane. The harmonic function $F(\nu_x, \nu_y)\exp[-j2\pi(\nu_x x + \nu_y y)]$ is regarded as a building block from which other functions may be composed by superposition. The variables ν_x and ν_y represent spatial frequencies in the x and y direction respectively. Thus when x and y have units of length (mm), ν_x and ν_y have units of cycles/mm. Components with spacial frequencies ν_x, ν_y , correspond to plane waves travelling at angles: $\theta_x = \sin^{-1}(\lambda\nu_x)$ and $\theta_y = \sin^{-1}(\lambda\nu_y)$. As shown in equation 2.6.1, $f(x,y)$ in space may be decomposed as a superposition integral of harmonic functions where the coefficients $F(\nu_x, \nu_y)$ are determined by the use of the two dimensional fourier transform as shown in equation 2.6.2 [3].

$$f(x, y) = \int_{-\infty}^{\infty} \int_{-\infty}^{\infty} F(v_x, v_y) \exp[-j2\pi(v_x x + v_y y)] dv_x dv_y \quad 2.6.1$$

$$F(v_x, v_y) = \int_{-\infty}^{\infty} \int_{-\infty}^{\infty} f(x, y) \exp[j2\pi(v_x x + v_y y)] dx dy \quad 2.6.2$$

Thus, taking the Fourier transform of $f(x,y)$, a distribution in space, gives $F(v_x, v_y)$, the distribution in the spatial frequency domain. Similarly, $f(x,y)$ can be obtained from $F(v_x, v_y)$ by taking the inverse Fourier transform of $F(v_x, v_y)$. In optics, a Fourier transform can be performed by a lens or by propagation into the far field.

2.7 Propagation Through Free Space : Fresnel Diffraction

Consider the harmonic input function $f(x,y) = A \exp[-j2\pi(v_x x + v_y y)]$ which corresponds to a plane wave $U(x,y,z) = A \exp[-j(k_x x + k_y y + k_z z)]$ where $k_x = 2\pi v_x$, $k_y = 2\pi v_y$, and $k_z = (k^2 - k_x^2 - k_y^2)^{1/2}$ or $k_z = 2\pi(1/\lambda^2 - v_x^2 - v_y^2)^{1/2}$. The output is $g(x,y) = A \exp[-j(k_x x + k_y y + k_z d)]$, where d is the distance travelled. The transfer function $H(v_x, v_y)$ is given by equation 2.7.1. Using the paraxial approximation, $\theta^2 = \theta_x^2 + \theta_y^2 \sim \lambda^2(v_x^2 + v_y^2)$, where θ is the angle with the optical axis, the phase factor is given by equation 2.7.2, which can be used to simplify $H(v_x, v_y)$, as shown in equation 2.7.3.

Using the Fresnel Approximation, the phase factor is a quadratic function of v_x and v_y and the output $g(x,y)$ can be determined from the input $f(x,y)$ in three steps. First, $F(v_x, v_y)$ is obtained by taking the Fourier transform of $f(x,y)$ as in equation 2.6.2. Next, we multiply $F(v_x, v_y)$ and $H(v_x, v_y)$ of equation 2.7.3 and the product gives the complex envelope of the plane wave components in the output plane. Taking the inverse Fourier transform of this product sums the contributions of all these plane waves and gives the output $g(x,y)$ as in equation 2.7.4 [3].

$$H(v_x, v_y) = \exp\left[-j2\pi \cdot \left(\frac{1}{\lambda^2} - v_x^2 - v_y^2\right)^{1/2} \cdot d\right] \quad 2.7.1$$

$$\text{PhaseFactor} = 2\pi \cdot \left(\frac{1}{\lambda^2} - v_x^2 - v_y^2\right)^{1/2} \cdot d = 2\pi \frac{d}{\lambda} (1 - \theta)^{1/2} \quad 2.7.2$$

$$H(v_x, v_y) = H_o \cdot \exp[j\pi\lambda d(v_x^2 + v_y^2)] \quad \text{where} \quad H_o = \exp[-jkd] \quad 2.7.3$$

$$g(x, y) = H_o \cdot \int_{-\infty}^{\infty} \int_{-\infty}^{\infty} F(v_x, v_y) (\exp[j\pi\lambda d(v_x^2 + v_y^2)] \cdot \exp[-j2\pi(v_x x + v_y y)]) dv_x dv_y \quad 2.7.4$$

This formulation is used to obtain the field distributions after successive round trips within the VIPA glass plate.

2.8 Propagation of a Beam Through a Lens

The plane wave components that constitute a wave can be separated by the use of a lens. A thin spherical lens transforms a plane wave into a paraboloidal wave focused to a point in the lens focal plane. If the plane wave arrives at small angles, θ_x and θ_y , the paraboloidal wave is centered about the point $(\theta_x f, \theta_y f)$, where f is the focal length. The lens therefore maps each direction (θ_x, θ_y) , into a single point $(\theta_x f, \theta_y f)$ in the focal plane and thus separates the contributions of the different plane waves [3].

As shown in figure 2-8-1 [3], let $f(x,y)$ be the complex amplitude of the optical wave in the $z=0$ plane. Light is decomposed into plane waves, with the wave travelling at small angles $\theta_x = \lambda v_x$, $\theta_y = \lambda v_y$, having a complex amplitude proportional to the fourier transform, $F(v_x, v_y)$. This wave is focused by the lens into a point (x,y) in the focal plane where, $x = \theta_x f = \lambda f v_x$, $y = \theta_y f = \lambda f v_y$. The complex amplitude at point (x,y) in the output plane is proportional to the fourier transform of $f(x,y)$ evaluated at 2.6.2 so that $g(x,y) \propto F(x/\lambda f, y/\lambda f)$. The coefficient of proportionality contains

a phase factor that is a quadratic function of x and y . Thus $g(x,y)$ is given by equation 2.8.1. If $d=f$, the phase factor vanishes and $g(x,y)$ is given by equation 2.8.2.

$$g(x, y) = h_1 \cdot \exp\left[j\pi \cdot \frac{(x^2 + y^2) \cdot (d - f)}{\lambda f^2}\right] \cdot F\left(\frac{x}{\lambda f}, \frac{y}{\lambda f}\right) \quad \text{where} \quad h_1 = \left(\frac{j}{\lambda f}\right) \cdot \exp[(-jk)(d + f)] \quad 2.8.1$$

$$g(x, y) = h_1 \cdot F\left(\frac{x}{\lambda f}, \frac{y}{\lambda f}\right) \quad \text{where} \quad h_1 = \left(\frac{j}{\lambda f}\right) \cdot \exp[(-jk)(2f)] \quad 2.8.2$$

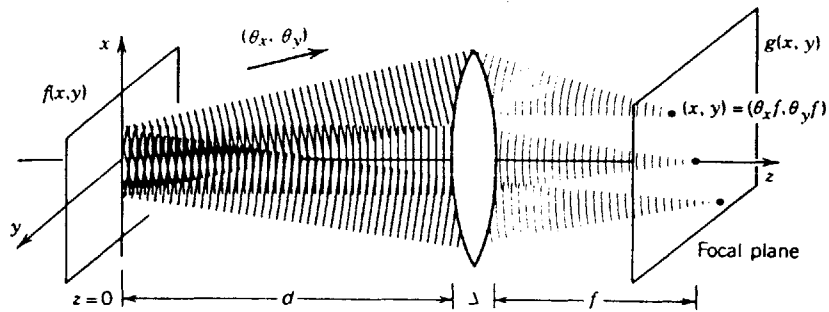


Figure 2-8-1 The complex amplitude $g(x,y)$ in the output plane is proportional to the fourier transform of $f(x,y)$

Chapter 3 VIPA Demultiplexing Method

This chapter describes the virtually imaged phase array (VIPA) technique as applied to an optical demultiplexer. This technique was developed by Dr. Masataka Shirasaki in 1995 at Fujitsu Labs [1]. Table 3-4 compares VIPA to other demultiplexing techniques in terms of angular dispersion, polarization dependence, economy of production, and other features.

3.1 Optical Demultiplexing Using VIPA

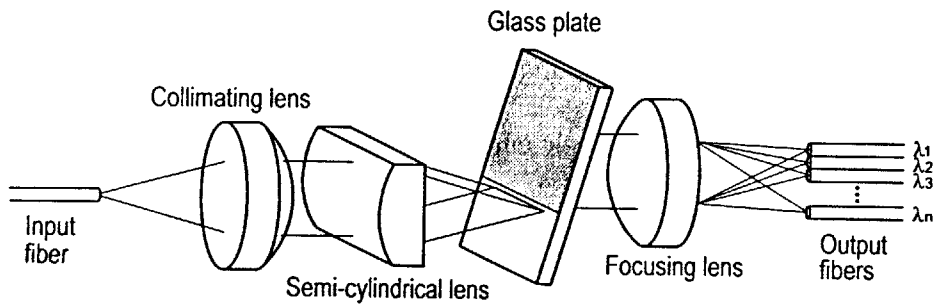


Figure 3-1-1 Schematic of VIPA system as a demultiplexer

Figure 3-1-1 shows a schematic of wavelength decomposition achieved with a VIPA. The system consists of a semi-cylindrical lens and a glass plate having coatings on both sides. The output of a single mode transmission fiber is passed through a collimating lens and this collimated light is the input to the VIPA. The input light is line focused into the glass plate using the semi-cylindrical lens. This light undergoes multiple reflections in the plate and emerges as collimated light from the reverse side of the plate. The output light propagates at an angle that varies with wavelength. In this way, the structure exhibits angular dispersion.

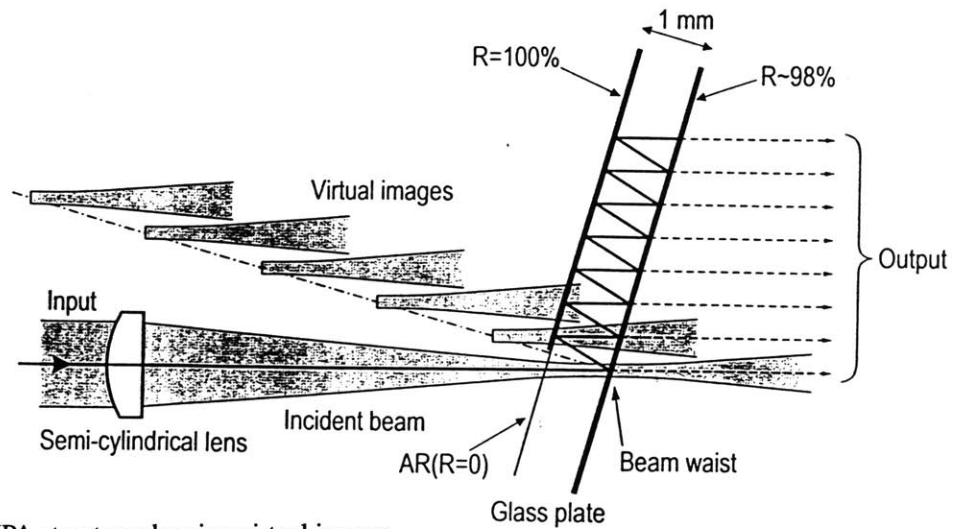


Figure 3-1-2 Detailed VIPA structure showing virtual images

Figure 3-1-2 shows in detail how the structure in fig 3-1-1. produces a virtually imaged phased array. The input side of the plate has 100% reflection coating, except in the incident light window area, which is anti-reflection coated. The output side of the plate has a high reflection coating of 95% or greater power reflectivity. After passing through the semi-cylindrical lens, the input light enters the window with a small incident angle and is line focused onto the surface of the output side. A small portion of the input light (5% or less in power) passes through the high reflection coating and diverges after the beam waist at the output surface. The rest of the light is reflected twice in the plate and returns to the output side, where another small portion of the remaining light passes through the high reflection coating and the rest of the light is reflected back into the glass plate.

In this way, the input light is split into many light-paths which have a constant displacement. Each light path has a beam that seems to be diverging from the beam waist created in the virtual image. These virtual images of the beam waist are self-aligned along the normal of the plate. If the effect of the refractive index of the glass ($n = 1.5$) on the transmission angles is neglected, then the vir-

tual images are spaced at distances equal to twice the plate thickness ($2t$), where t is the thickness of the glass plate.

The output light corresponds to that produced by a phased array of sources, whose diverging beams interfere to produce angularly dispersed, collimated light. The output light of the glass plate is passed through a focusing lens and the intensity peaks of the different wavelengths are then coupled to fibers placed at appropriate positions.

3.2 Angular Dispersion

The beams transmitted through the glass plate interfere such that light propagates in a direction that varies with the wavelength of the light. The spacing of the light paths is $d=2t \sin(\theta)$, where t is the plate thickness and θ is the incident angle. The difference in the path lengths between adjacent beams is $2t \cos\theta$. The angular dispersion is the ratio of these two numbers which is $\cot\theta$ and after the plate, it is $\sim n$ times larger due to refraction. Thus the effective factor that determines the dispersion is approximately $n \cot\theta$. For experiments using the $1.55\mu\text{m}$ wavelength range, $t=100\mu\text{m}$, $\theta= 6.4$ degrees, $d=22.4\mu\text{m}$, the factor $n \cot\theta$ is 13.4 [1]. A similar factor for a diffraction grating is given by $2\tan(\text{blaze angle})$ and this factor for a common blaze angle of 30 degrees is ~ 1 . Thus the angular dispersion of the VIPA is much larger than those of the gratings.

3.3 Polarization Dependence

The VIPA is essentially insensitive to the polarization state of the input light. Polarization dependence appears only if the complex reflectivities of the reflection films have polarization dependence in either amplitude or phase. Polarization dependence can be ignored for a small incident angle below ten degrees.

3.4 Comparison of VIPA with other Demultiplexers

Table 3-4. Comparison of VIPA to Other Demultiplexers

Demux	app to DWDM	Angular Dispersion	Polarization Dependence	Other
Fabry- Perot Mach-Zehnder Interferometers	must cascade & allign many filters		Pol. Dep. can be eliminated	cost increases with number of channels
Diffraction Gratings	parallel demultiplexing	$2*\tan(\text{blazeang})$ $\sim 2* \tan(30)$ ~ 1	Diffraction Efficiency depends on I.P.S	
Waveguide Diff. Gratings (Dragone Filter)	parallel demultiplexing	better ang. disp ~ 10	Pol. Dep. can be eliminated	Stability Problems
VIPA	parallel demultiplexing	large. ang. disp. $n*\cot(\text{inc.ang.})$ ~ 13.4 10-20 times greater than Diff. Gratings	For small inc. angles (<10), no/lo dependence on I.P.S	compact, simple, low cost,

Unlike Fabry Perot interferometers, where multiple filters must be cascaded and alligned, the VIPA uses parallel demultiplexing. As discussed in section 3.2, the angular dispersion of the VIPA system is about 10 to 20 times greater than that of diffraction gratings and is also considerably greater than that of waveguide gratings. Section 3.3 explained VIPA's no/low dependence on input polarization state, which is a big advantage over diffraction gratings whose diffraction efficiency depends on the input polarization state. Finally, the VIPA system is free from the stability problems encountered by Waveguide Diffraction Gratings and is compact, simple and low cost.

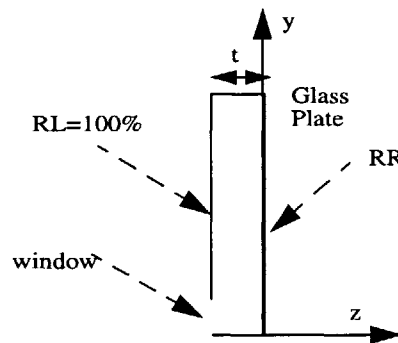
Chapter 4 The VIPA Simulation Model

This chapter presents a mathematical formulation of the VIPA demultiplexing system based on Fourier optics. The simulation implements this model in Matlab. This chapter also describes methods used to assess the performance of the VIPA demultiplexer and explains how various VIPA parameters are optimized to improve its performance.

4.1 Computing VIPA Field Distributions

A two dimensional model, as in figure 4-1-1, is used to describe the orientation of the glass plate, electric field distributions, incident angle, surface reflectivities and other relevant parameters of the VIPA system. The output side of the glass plate is aligned with the y axis and the bottom of the plate runs along the z axis. The field distributions along x are identical to the those along y and so it was sufficient to use a 2-D model to analyze the VIPA system.

Figure 4-1-1 Base coordinate system and glass plate of thickness t , with output side along y.



RL and RR are defined as the reflectivity amplitude distributions, as a function of y , along the left and right surfaces, respectively. From RL and RR , we can compute the following other useful parameters as follows.

1. **Table 4-1: Expressions for Reflection and Transmission profiles for $y \geq y_0$**

Parameter	left boundary of Plate	right boundary of Plate
Amplitude Reflectivity	$R_L = 1$	R_R
Power Reflectivity	$r_L = R_L^2 = 1$	$r_R = R_R^2$
Power Transmissivity	$t_L = 1 - r_L = 0$	$t_R = 1 - r_R$
Amplitude Transmissivity	$T_L = \sqrt{t_L} = 0$	$T_R = \sqrt{t_R}$

The incident beam enters the glass slab through a small window on the lower left side. The window extends from the bottom of the glass slab, $y=0$ to $y = y_0$ ($y_0 = 50 \mu\text{m}$) along the left boundary of the slab ($z = -t$) and within the window region, R_L is 0, and T_L is 1. Beyond $y=y_0$, $R_L=1$, that is, above the window, the left side is perfectly reflective. R_R and T_R , the reflectivity and transmissivity profiles along the right side depend on the specific VIPA design.

Two different VIPA designs are simulated. The basic VIPA model uses a glass plate with uniform reflectivity and transmissivity along the right boundary. In the improved VIPA model, the right side of the plate has varying transmissivity and reflectivity profile. In the basic model, the right side usually has high uniform reflectivity of $r_R \geq 95\%$ such that a small fraction of the incident field ($\leq 5\%$ of the power) is transmitted through. The improved model is simulated for the case where t_R increases linearly from 0 to 1 over the range $y=y_0$ to the top of the plate.

Section 2.4 explains why the input to the glass plate can be approximated as a gaussian beam. Let E_{in} be the electric field distribution of the input gaussian beam, described along the y axis. E_{in} enters the glass slab through the window, at an incident angle of θ_{air} in air. It undergoes refraction at the air-glass boundary and is incident on the right boundary at an angle of θ_{glass} . ($= \theta_{air}/n$). At this point of incidence, ($y= y_0, z=0$), the beam has its smallest spot size, with beamwaist, W_0 . The

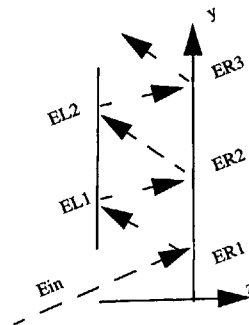
field at this position is called ER_1 . Since E_{in} enters at a nonzero angle of incidence, its phase is linear and is given by $\exp(j(y - y_o)k_{yglass})$, where k_{yglass} is the y component of the propagation constant in glass, $k = 2\pi/\lambda_g$, and $\lambda_g = \lambda/n$ is the wavelength in glass. Equation 4.1.1 gives the complete expression for ER_1 , the gaussian beam distribution along y at the point of incidence.

$$ER_1 = A_o e^{-\left(\frac{(y - y_o)^2}{W_o^2}\right)} e^{j(y - y_o)k_{yglass}} \quad 4.1.1$$

In most cases, $A_o = 1$ and $y_o = 50\mu\text{m}$. The beam waist, W_o , depends on the wavelength, incident angle and plate thickness, t .

Now we will follow the beam as it reflects off the right boundary and travels through the length of the slab and will examine its profile just before it hits each side of the plate. N is the pre-specified number of reflections that the beam undergoes and is usually set to 200. The length of the glass plate must be long enough to accommodate the field after the N th reflection. As shown in figure 4-1-2, EL_i ($i = 1, 2, \dots, N$) designates the field profiles along the left side, just as they arrive at the left boundary from the right side, before they have undergone reflection. Similarly, all fields on the right side are labelled, ER_i ($i = 1, 2, \dots, N$). These describe the profiles just before they are reflected or transmitted from the right boundary of the plate. All angles of incidence and reflection, on either side, are equal to θ_{glass} .

Figure 4-1-2 Beam positions inside the glass plate after successive reflections at each boundary.



At this point, we assume that the entire field, E_{in} enters through the window and that no power is lost due to the finite extent of the window. This assumption will be modified later, in section 4.2. We will also ignore any power escaping through the window when the field hits the left side.

When ER_1 hits the right boundary, most of its power is reflected and a small fraction is transmitted. Thus when ER_1 reflects off the right boundary, its amplitude is scaled by RR . The scaled version of ER_1 , then propagates from the right to the left side through a distance equal to $t \cdot \cos \theta_{glass}$, to give EL_1 . After EL_1 is perfectly reflected from the left boundary, it travels to the right at an angle of θ_{glass} , through an equal distance of $t \cdot \cos \theta_{glass}$, in the opposite direction, to produce ER_2 . In this way, the beam undergoes repeated reflections and propagations as it travels through the glass plate.

As discussed in section 2.4.4, Fourier optics is used to compute the transformations of the gaussian beams as they propagate through glass. Let VL_i be the Fourier transforms of EL_i and VR_i be the Fourier transforms of ER_i , for $i= 1,2,3,\dots,N$, respectively. When Propagating through glass of refractive index $n= 1.5$ through a distance, $t \cdot \cos \theta_{glass}$, in the positive z direction, the propagation phase factor is given by PR as in equation 4.1.2. For propagation through the glass plate, through an equal distance in the negative z direction, the propagation phase factor is given by PL , as in equation 4.1.3. Using these we can obtain ER_i from EL_{i-1} , and EL_i from ER_i , for $i=1,2,\dots,N$.

$$PR = e^{ik_{glass}t \left(1 - \frac{1}{2} \left(\frac{k_{yglass}}{k_{glass}}\right)^2\right)} \quad 4.1.2$$

$$PL = e^{ik_{glass}(-t) \left(1 - \frac{1}{2} \left(\frac{k_{yglass}}{k_{glass}}\right)^2\right)} \quad 4.1.3$$

The simulation computes EL_1 from ER_1 according to equation 4.1.4, and then uses EL_1 to compute ER_2 as in equation 4.1.5. In this way it computes all profiles, EL_i, ER_i , for a specified number of reflections, N .

$$EL_1 = F^{-1}\{F(RR \cdot ER_1) \cdot PL\} \quad 4.1.4$$

$$ER_2 = F^{-1}\{F(RL \cdot EL_1) \cdot PR\} \quad 4.1.5$$

$$EL_i = F^{-1}\{F(RR \cdot ER_i) \cdot PL\} \quad 4.1.6$$

$$ER_i = F^{-1}\{F(RL \cdot EL_{i-1}) \cdot PR\} \quad 4.1.7$$

Having described the electric field profiles within the glass plate, I now compute the output profiles produced by the fields transmitted through the right side of the plate. Recall that the left boundary is perfectly reflective ($RL=1$) and so no energy is transmitted through the left side. On the right surface, the transmissivity is given by, $tR = j \sqrt{1-RR} = \exp(\pi/2) * \sqrt{1-RR}$. The transmitted fields ET_i are the transmitted portion of the fields ER_i . Thus ET_i is a scaled and phase shifted form of ER_i and is also gaussian.

Using the above method, the simulation obtains the transmitted fields ET_i from the previously computed profiles ER_i , for $i = 1, 2, \dots, N$, by equation 4.1.8. To obtain the total field transmitted through the glass plate, ET_{total} , we simply use superposition and sum over all transmitted profiles, ET_i , as shown in equation 4.1.9.

$$ET_i = jTR \cdot ER_i \quad 4.1.8$$

$$ET_{total} = \sum_{i=1}^N TR_i \quad 4.1.9$$

The total electric field, ET_{total} , then passes through a spherical lens of focal length f and diameter d , to give the far field pattern, VT_{total} . As described in section 2.4.5, passing a beam through a lens from one focal plane to another, is equivalent to taking the Fourier transform of the beam. Thus VT_{total} is computed by taking the Fourier transform of the field ET_{total} .

While the beams inside the slab are always gaussian, the output field profiles depend on the reflection/transmission profiles along the right boundary. For the basic VIPA design with uniform transmissivity, ET_{total} has exponentially declining magnitude and linear phase and consequently, VT_{total} is Lorentzian with symmetric amplitude and anti-symmetric phase. The modified VIPA design with linear transmissivity leads to more symmetric output field patterns.

The variable, axis_pts , denotes the number of points used to describe the field profiles along y . Generally axis_pts is set to $1024*8$ for a plate of length $2050\mu\text{m}$. This provides a resolution of $\sim 0.25\mu\text{m}$, which is sufficient for most fields. However, to obtain a smoother distribution of VT_{total} , a zero padded Fourier transform of ET_{total} was performed using 4 times as many points.

The far field pattern, VT_{total} , of the VIPA output consists of multiple lobes. The receiving output fiber is then aligned with the main lobe so that the energy of VT_{total} can be coupled to the output fiber.

4.2 Power Loss at Window of Glass Plate:

The window of the glass plate is of finite size and extends from $0 \leq y \leq y_0$. However, the tails of the gaussian field entering through the window extend beyond the window limits. Hence some of the incident power is lost upon entry through the window and the beam undergoes some distortion. The extent of power lost depends on the width of the gaussian at the window and also on the incident angle of the gaussian. Optimization of the plate thickness, beamwaist size and incident angle to minimize power loss at the window is discussed in a later section. Here I describe how the simulation accounts for this power loss.

Though the E field incident upon the left boundary is an ideal gaussian, after passing through the window, the field incident upon the right boundary, called ER_1 , is not a true gaussian, but one that has its tails cut off abruptly. Rather than starting with a deformed gaussian, the simulation uses an indirect method to obtain an accurate model of the field at ER_1 . This is described below using figure 4-2-1. We start with an ideal gaussian, ER_{ideal} , with linear phase, at the point of incidence ($z=0$ and $y=y_0$), corresponding to ER_1 described earlier, given by the expression in equation 4.2.1.

Figure 4-2-1 (a) shows she magnitude and phase profile of ER_{ideal} .

$$ER_{ideal} = ER_1 = A_o e^{-\left(\frac{(y-y_0)^2}{W_o^2}\right)} e^{i(y-y_0)k_{y, glass}} \quad 4.2.1$$

$$EL_{ideal} = F^{-1}\{F\{ER_{ideal}\} \cdot PL\} \quad 4.2.2$$

$$EL_{mod} = EL_{ideal} \cdot (1 - RL) \quad 4.2.3$$

$$ER_{mod} = F^{-1}\{F\{EL_{mod}\} \cdot PR\} \quad 4.2.4$$

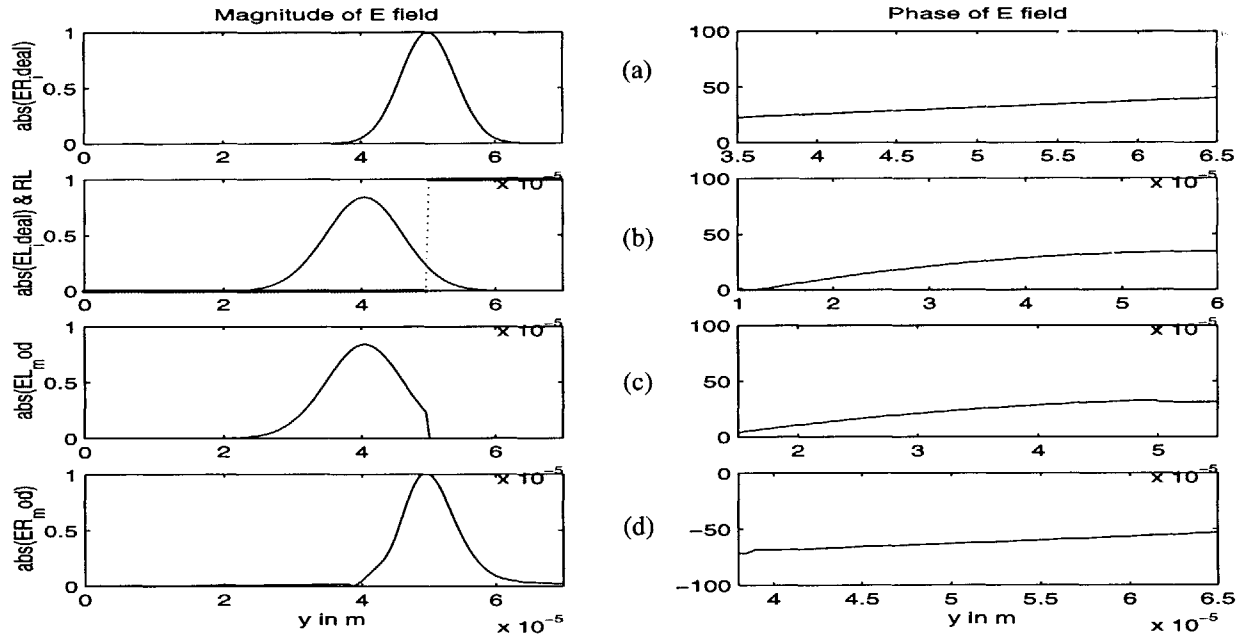


Figure 4-2-1 Illustration of power loss at window. (a) magnitude and phase of ideal beam at point of incidence. (b) profiles of ideal beam at window, on left boundary. (c) profiles at window with truncated tails due to window (d) truncated beam at point of incidence that represents beam after power loss at window.

Now using, PL (propagation phase factor from right to left), we retrace the path followed by the incident beam, to obtain, EL_{ideal} , the ideal gaussian at the left boundary, just after it has entered the window with no power loss. Using the previous method of propagation through glass, EL_{ideal} is computed as shown in equation 4.2.2. and appears in figure 4-2-1 (b).

Now EL_{ideal} is multiplied by the inverse reflectivity profile, RL_{inv} , of the left boundary (RL). Thus, $RL_{inv} = 1$ over the region of the window, $0 < y < 50\mu m$, and $RL_{inv} = 0$, $y > 50\mu m$. This removes the section of the incoming gaussian that does not pass through the window. The new modified profile, in the same position as EL_{ideal} , is called EL_{mod} , and EL_{mod} is given by equation 4.2.3 and is shown in figure 4-2-1(c). EL_{mod} is an accurate version of the gaussian just after it enters through the window. EL_{mod} then propagates to the right, at an angle of θ_{glass} , through a distance of $t \cdot \cos\theta_{glass}$ to give, ER_{mod} , as in equation 4.2.4. ER_{mod} appears as a very slightly distorted version of ER_{ideal} in figure 4-2-1(d). ER_1 described previously is set equal to ER_{mod} and the simulation then computes the rest of the profiles as the beam propagates through the length of the glass plate.

4.3 Optimizing Beam Waist Size, Window Size, and Incident Angle

The presence of a finite window leads to power loss upon entry of the beam through the window and also when the beams impinge on the left surface. Power loss at the window depends on the beam width of the gaussian at the window relative to the size of the window and also on the angle of incidence of the beam.

We would like to make the incident angle as small as possible. To maximize the energy entering the window, it is desirable to minimize the beam width at the window. In general, the beam width $W(z)$ of a gaussian beam at a certain distance, z , from the beam waist, W_o , is given by equation 4.3.1. The distance of the window from the point of incidence is $t \cdot \cos \theta_{\text{glass}}$, which, for small values of θ_{glass} , can be approximated to t , the thickness of the glass plate. Thus the width of the gaussian at the window, W_{window} , is given by eqn 4.3.2:

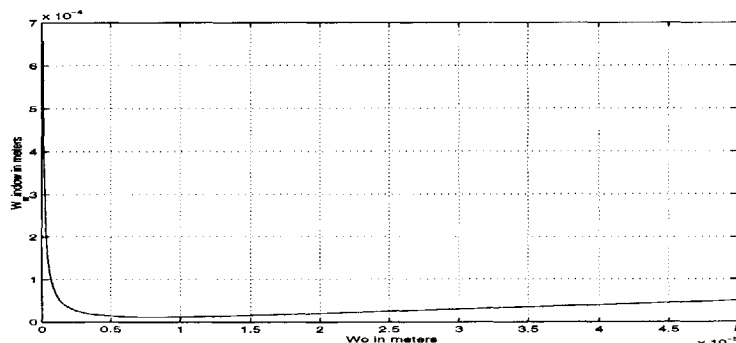
$$W(z) = W_o^2 \cdot \left[1 + \left(\frac{\lambda_g \cdot z}{\pi \cdot W_o} \right)^2 \right]^{1/2} \quad 4.3.1$$

$$W_{\text{window}} = W_o \cdot \sqrt{1 + \left(\frac{2 \cdot t}{z_o} \right)^2} \quad \text{where} \quad z_o = \frac{\pi \cdot W_o^2}{\lambda/n} \quad 4.3.2$$

$$W_{o-\text{opt}} = \sqrt{\frac{\lambda_g \cdot t}{\pi}} \quad 4.3.3$$

Figure 4-3-1 shows how W_{window} varies with W_o for $t=100\mu\text{m}$, $\lambda=1550\text{nm}$, and $n=1.5$. For these parameters, the graph shows that W_{window} achieves its minimum value for $W_o=5.64\mu\text{m}$. In general, we can obtain an expression for W_o in terms of wavelength λ , and thickness t , that minimizes $W(z)$. This is done by minimizing the expression for $W(z)$ in eqn 4.3.1 with respect to W_o . In other words, the derivative of $W(z)$ w.r.t. W_o is set to zero and is solved for W_o . The result is the optimal beam waist size, $W_{o-\text{opt}}$, for a certain wavelength and plate thickness, as given in equation 4.3.2. Thus, for a given wavelength in glass, λ_{glass} , and a certain plate thickness, t , the above expression gives the beam waist, $W_{o-\text{opt}}$ that minimizes the gaussian beam width at the window.

Figure 4-3-1 Graph of beam width at window, W_{window} versus beam waist, W_o for $t=100\mu\text{m}$, $\lambda = 1550\text{nm}$. W_{window} is minimum for $W_o=5.64\mu\text{m}$



4.4 Overall Efficiency of VIPA System

The collimated light from the glass plate is focused onto output fibers. The overall efficiency of the system is measured as the fraction of the input power that is successfully transferred to the output fibers. The three main sources of loss in the system are:

- power lost at the input window of the glass plate
- power lost to side lobes of the output field
- imperfect coupling of main lobe of output field to the output fiber.

The simulation can compute these losses and the relevant VIPA parameters can be adjusted to minimize the total loss and hence maximize the power efficiency of the system. Total efficiency is the product of three factors as follows: $\text{Efficiency} = W * M * C$ where

$W = 1 - \text{power lost at window}$,

$M = \text{fraction of energy of output field in main lobe}$

$C = \text{coupling efficiency of main lobe to output fiber mode.}$

Optimizing parameters to maximize the power efficiency is an iterative process, as there are trade-offs among power losses at the different stages. For example decreasing the incident angle, decreases power lost at window but increases power lost to side lobes of the output field. Thus rather than maximizing W , M , and C independently, parameters are chosen to maximize the product of W , M , and C so as to achieve highest overall efficiency.

4.4.1 Power Loss at Window

To compute the power loss at the window, for a given wavelength, plate thickness, refractive index, and incident angle, we first compute the optimal beam waist size by the method described

above. According to section 4.3, the optimum beam waist at the point of incidence is given by eqn 4.3.2, and the corresponding optimum beam width at the window is given by eqn 4.3.3. W_{window} is the beam width of the amplitude profile. The power distribution is the square of the amplitude distribution and the width of the power profile, W_{power} is given by $W_{\text{window}}/\sqrt{2}$. The fraction of this power profile cut off by the window is computed using the error function, which is performed in matlab using the 'erf' command. The distance between the power profile center and the window edge is an offset given by eqn 4.4.1a. The matlab function, erf, then uses this offset to compute the power loss in percent according to eqn 4.4.1b [7].

$$\text{offset} = 100 \cdot 10^{-6} \cdot \tan(\pi \cdot \theta) \quad 4.4.1a$$

$$W = \left(100 \cdot \left(1 - \text{erf}\left(\frac{\text{offset}}{W_{\text{power}} \cdot \sqrt{2}}\right) \right) \right) / 2 \quad 4.4.1b$$

Rather than setting the incident angle and computing the resultant window power loss (1-W), as discussed above, the simulation sets the loss at the window and computes the corresponding incident angle, for a given plate thickness, center wavelength, and refractive index. The optimal beam waist is computed as in section 4.3 and the matlab command, 'erfinv' is used, as in equation 4.4.1c, to perform the inverse error function computation that provides the offset corresponding to the desired window power loss. The incident angle in air is then calculated from this offset value by eqn 4.4.1d.

$$\text{offset} = \text{erfinv}(1 - W^2) \cdot W_{\text{power}} \cdot \sqrt{2} \quad 4.4.1c$$

$$\theta_{\text{air}} = \text{atan}\left(\frac{\text{offset}}{100 \cdot 10^{-6}}\right) \cdot \frac{180}{\pi} \quad 4.4.1d$$

4.4.2 Power Loss to Side Lobes

The far field pattern V_{Ttotal} of the VIPA output consists of multiple lobes. As only the main lobe is coupled to the output fiber, it is important to minimize the energy of the side lobes. The simula-

tion computes M , which is the ratio of energy in the mainlobe to the energy of the entire far field pattern. The main lobe is identified by seeking the position of maximum value of the power profile using the matlab command ‘max’ and then selecting a proper range of points from the power profile around this maximum. Discrete integration is used to compute M , according to equation 4.4.1e, where Δky is the interval between points of the ky vector and $axis_pts$ is the number of points used to define field and ky vectors.

$$M = \frac{\Delta ky \cdot \sum_{max-100}^{max+100} VTtotal}{\Delta ky \cdot \sum_1^{axispts} VTtotal} \quad 4.4.1e$$

Energy distribution among the lobes is affected primarily by the incident angle. Decreasing the angle of incidence reduces the power lost to side lobes but increases the power lost at the window and thus there is a trade-off between W and M .

4.4.3 Coupling Efficiency:

It is important to evaluate the coupling efficiency of the main lobe of the far field pattern to the gaussian mode of the output fiber. The beam profile along x , which is the direction perpendicular to the y - z plane of our 2-D model, is assumed to be gaussian. When the output light is focused onto a gaussian mode using a lens, the coupling efficiency is calculated from the square of the overlap integral between the focused beam and the gaussian mode of the output fiber.

To maximize the power transferred from the main lobe of the field to the output fiber, the position of the fiber along y and its radius must be adjusted. This is equivalent to maximizing the coupling efficiency between the main lobe of the field, $VTtotal$, and a gaussian mode by adjusting the peak, amplitude position and width of the gaussian mode.

To illustrate how this is done in the simulation, let E_v be the main lobe of the far field output, V_{Total} , and let E_f be the gaussian mode of the fiber. Equation 4.4.3a shows the general form of E_f .

$$E_f = A_f \cdot e^{-\left\{ \frac{(ky - ky_f)^2}{W_f^2} \right\}} \quad 4.4.3a$$

The gaussian mode parameters, A_f (peak magnitude), ky_f (position of peak), and W_f (width of the fiber mode) must be chosen, by a process of iteration and inspection, to maximize the coupling efficiency between E_v and E_f . Starting with an initial approximation of E_f , I first try to match the magnitude profiles of E_v and E_f as best as possible. A_f is set equal to the peak of the magnitude profile of E_v , and ky_f is set equal to the position of this peak. The matlab command, `max`, gives the peak value of the magnitude of E_v and its corresponding Ky value. However, the discrete nature of E_v limits accuracy, as the values given by `max` may not be at the true peak of the continuous curve. As E_v is not a true gaussian, there is no straight forward way to calculate W_f and so it is optimized by inspection and iteration until the best overlap is obtained between E_v and E_f .

The presence of a linear or other non uniform phase in E_v leads to low coupling efficiency. A linear phase term can be removed by changing the position of the focusing lens so that a phase factor, $\exp(j*PPL*ky)$, cancels the linear phase of E_v , $\exp(j*PPv*ky)$. The slope of the linear phase of E_v , PPv , is estimated from the phase profile of E_v . PPL is then set equal to $-PPv$. The passage of E_v through a lens of phase factor ($PPL = -PPv$) is performed numerically by equation 4.4.3 b and c. If $PPL = -PPv$ exactly, then $E_v' = |E_v|$ which has a uniform phase

Before Lens $E_v = |E_v| \cdot e^{(i \cdot PPv \cdot ky)}$ 4.4.3b

After Lens $E_v' = |E_v| \cdot e^{(i \cdot PPv \cdot ky)} \cdot e^{(i \cdot PPl \cdot ky)}$ 4.4.3c

Now we calculate the coupling efficiency between E_v' (E_v after phase adjusting lens) and E_f , the gaussian fiber mode constructed previously. E_v' and E_f are both normalized to give \bar{E}_v' and \bar{E}_f respectively, and these are computed according to equations 4.4.3d and e.

$$\bar{E}_v' = \frac{E_v'}{\sqrt{\int |E_v'|^2 dk y}} = \frac{E_v'}{\sqrt{\Delta k y \cdot \sum |E_v'|^2}} \quad 4.4.3d$$

$$\bar{E}_f = \frac{E_f}{\sqrt{\int |E_f|^2 dk y}} = \frac{E_f}{\sqrt{\Delta k y \cdot \sum |E_f|^2}} \quad 4.4.3e$$

The coupling efficiency, C , is then given by equation 4.4.3f. As E_f is purely real, $\text{conj}(\bar{E}_f) = \bar{E}_f$ and C can be simplified as shown in 4.4.3f.

$$C = \left| \int (\bar{E}_v' \cdot (\bar{E}_f)^*) dk y \right|^2 = \left| \Delta k y \cdot \sum (\bar{E}_v' \cdot \bar{E}_f) \right|^2 \quad 4.4.3f$$

4.5 Multi-wavelength input

The previous sections describe the numerical procedures used to calculate the output field produced by one particular wavelength. This model is easily extended to the case of input containing multiple wavelengths. For multi-wavelength input, the simulation uses the same mathematical formulations to compute the output produced by each wavelength. Thus using an input of ten different wavelengths is equivalent to running the above simulation separately for each of the ten wavelengths. Instead of doing this, the simulation stores the parameters and outputs of each wavelength in separate arrays, so that the output of the ten wavelengths can be viewed together so as to emulate the parallel demultiplexing feature of the VIPA system. If multiple wavelengths are used, a single wavelength is specified, and this is used to perform efficiency calculations. Usually, wavelengths are centered around 1550nm and the 1550nm wavelength input is used to perform efficiency calculations.

Chapter 5 Simulation Results

This chapter presents the simulation results of the VIPA demultiplexing system. It compares the performance of the two main VIPA designs: the basic design using a glass plate with uniform transmissivity and the improved design whose glass plate has a coating of linearly varying transmissivity. Sections 5.1 and 5.2 present results of single wavelength input for the two VIPA designs respectively. In 5.3, I discuss features of the output produced by multi-wavelength input, and how changes in VIPA parameters effect field distributions and system efficiency.

5.1 VIPA with Uniform Transmissivity

This section presents the simulation results of the basic VIPA demultiplexer that uses a glass plate with uniform reflectivity and transmissivity along its right boundary. Results are presented for the case of power reflectivity, rR , equal to 95%, and power transmissivity, tR , equal to 5%.

5.1.1 Field Profiles Inside Glass Plate

Figure 5-1 shows the electric field profiles of the beam at various positions along the right side of the glass plate. All fields were produced by running the simulation for a single wavelength input of 1550nm. For a plate of thickness of 100 μm and window power loss of 1%, the corresponding optimized parameters are: beam waist of 5.7 μm , and incident angle 7.7 degrees. The plots illustrate the beam at six positions ER_1 , ER_2 , ER_3 , ER_5 , ER_{10} , ER_{15} , along the right side of the glass plate, as described in section 4.1

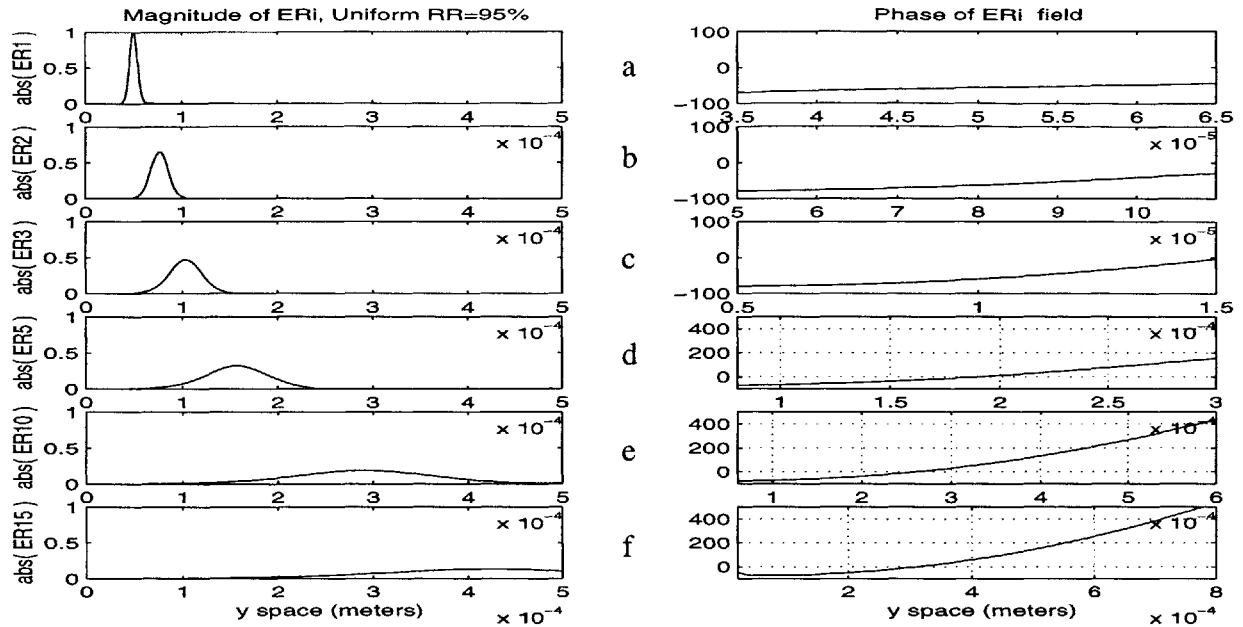


Fig 5-1 Magnitude and phase profiles of E fields of beam along y, in glass plate, just before reflection at each boundary. (a) profile of beam at point of incidence (ER_1); (b) profile of beam at (ER_2); (c) profile of beam at (ER_3); (d) profile of beam at (ER_5); (e) profile of beam at (ER_{10}); (f) profile of beam at (ER_{15}).

In figure 5-1, The plots in the left column show the field magnitudes of the beams along y, at each position. The corresponding phase profiles appear in the right column. The first row describes ER_1 , which is the beam at its point of incidence on the right side of the plate. As expected, the beam has a gaussian magnitude profile, with unity peak occurring at $y=50\mu\text{m}$ and has a one sided beam width of $\sim 5.7\mu\text{m}$. Its phase is purely linear due a nonzero angle of incidence. ER_2 describes the beam after one round trip through the plate, just before its second reflection on the right boundary. From the plots in the second row, we see that ER_2 has a lower magnitude and greater beam width than ER_1 and also that ER_2 has a parabolic phase component. At ER_3 , the beam is just about to undergo its third reflection at the right boundary. The beam at ER_3 is wider and has a lower peak than that of ER_2 . Its parabolic phase has a greater curvature as it has travelled through a greater distance of glass. ER_5 , ER_{10} , and ER_{15} describe the beam immediately before its fifth,

tenth and fifteenth reflection, respectively, on the right boundary. These graphs illustrate how the beam progressively spreads and diminishes in magnitude and how its phase curvature increases as it travels through the glass plate.

5.1.2 Output Field Profiles

For the basic model with uniform transmissivity, the output field distribution can be derived analytically as follows. The decay rate in one round trip is the square root of the reflectivity, which is ~ 0.975 when the constant reflectivity is 95%. Under the conditions that the reflectivity has no phase and does not vary in the range of the incident angle, the beam profiles in all the light paths are the same because they are virtual images. Assuming that the field magnitude in a beam is constant around the output peak direction, the output field traveling in the direction of angle $\Delta\phi$, is proportional to $1/[1 - \exp(-\alpha + j\Delta\phi kd)]$, where $\Delta\phi$ is the small deviation in radians from the Bragg angle; $\exp(-\alpha)$ is the decay rate in the VIPA; k is the propagation constant, $2\pi/\lambda$; and λ is wavelength. The approximation is valid for small α and small $k*d*\Delta\phi$. Thus the far field pattern of the output light is Lorentzian

As described in section 4., the field just outside the glass plate, T_{total} , is sum of the fields transmitted through the plate every time the beam hits the right boundary. According to the above analysis, T_{total} should decay exponentially along y . Figure 5-2, is a plot of the magnitude and phase of the output field, T_{total} , along y , just outside the glass plate, for a single wavelength input of 1550nm and the parameters specified in section 5.1.1. This curve is very unsmooth as it contains components of the output light travelling in all directions. A modified version of this output field is described later in fig 5-3.

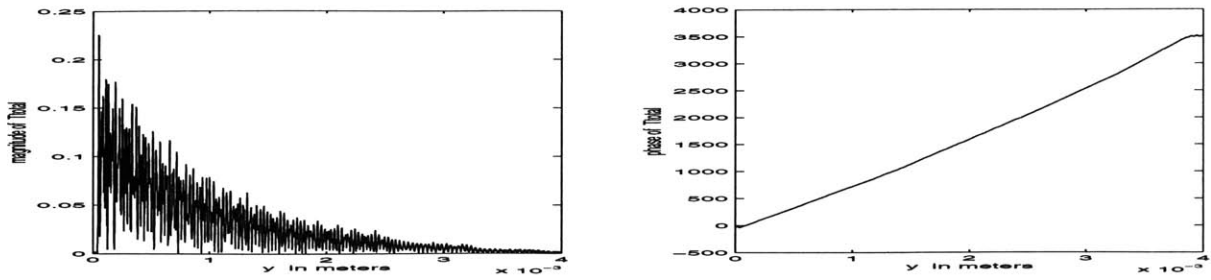


Figure 5-2 Magnitude (left) and phase(right) profiles of total output field T_{total} , along y , just outside glass plate. Note linear phase and exponentially decaying magnitude.

The output from the glass plate, T_{total} , passes through a spherical lens to produce focused beams, V_{total} , that can be coupled to output fibers. V_{total} is computed by taking the Fourier transform of T_{total} , as discussed in section 4. T_{total} has an exponential profile and thus its Fourier transform, V_{total} , is Lorentzian. Figure 5-3 shows the focused pattern, V_{total} , along the spatial frequency y component, produced by the same input and glass plate parameters as described in 5.1.1. A zero padded Fourier transform of T_{total} is computed to obtain a smoother curve.

This output field contains four distinct lobes, which have been labelled as 1,2,3,4, from low to high k_y values. The lobes are produced by the different components of light in T_{total} travelling in different directions. Each of these lobes has a Lorentzian field distribution. The main lobe is identified as the one with highest maximum amplitude and in figure 5-3, lobe 2 is the mainlobe. The mainlobe peaks at $k_y \sim 7.6 * 10^5$ rad/sec. The mainlobe is produced by the component of T_{total}

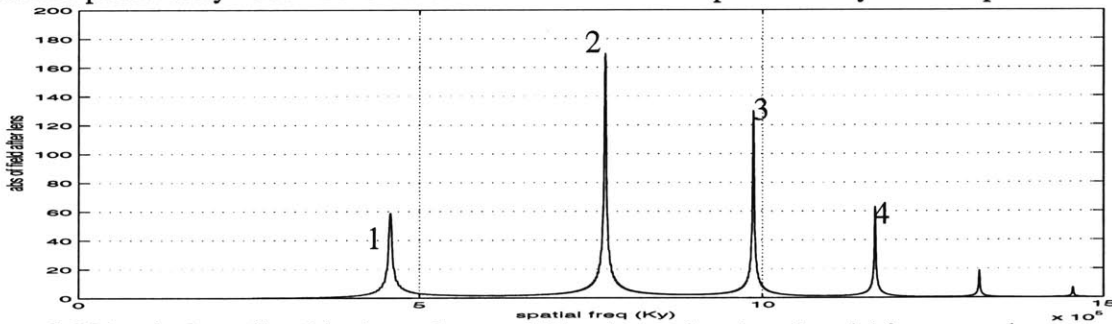


Figure 5-3 Magnitude profile of the focused pattern V_{total} , as a function of spatial frequency along y . Lobes are Lorentzian and are numbered 1,2,3,4. Lobe 2 is the main lobe while the rest are side lobes.

that travels straight through, at an angle closest to the incident angle. This output field has many interesting features.

The envelope curve, formed by the peakvalues of the individual lobes, is itself a gaussian, which is expected as the input field is a gaussian. This fact becomes more obvious in fig 5-2-1-2, where we observe the output of numerous wavelengths together.

In figure 5-3, we see that the distance between lobes 1 and 2 is greater than that between lobes 2 and 3, which is in turn greater than that between lobes 3 and 4. Thus the spacing between lobes decreases as k_y increases and this is true for all wavelengths and incident angles. These and other features will be described further when the multi wavelength output is presented in section 5-3.

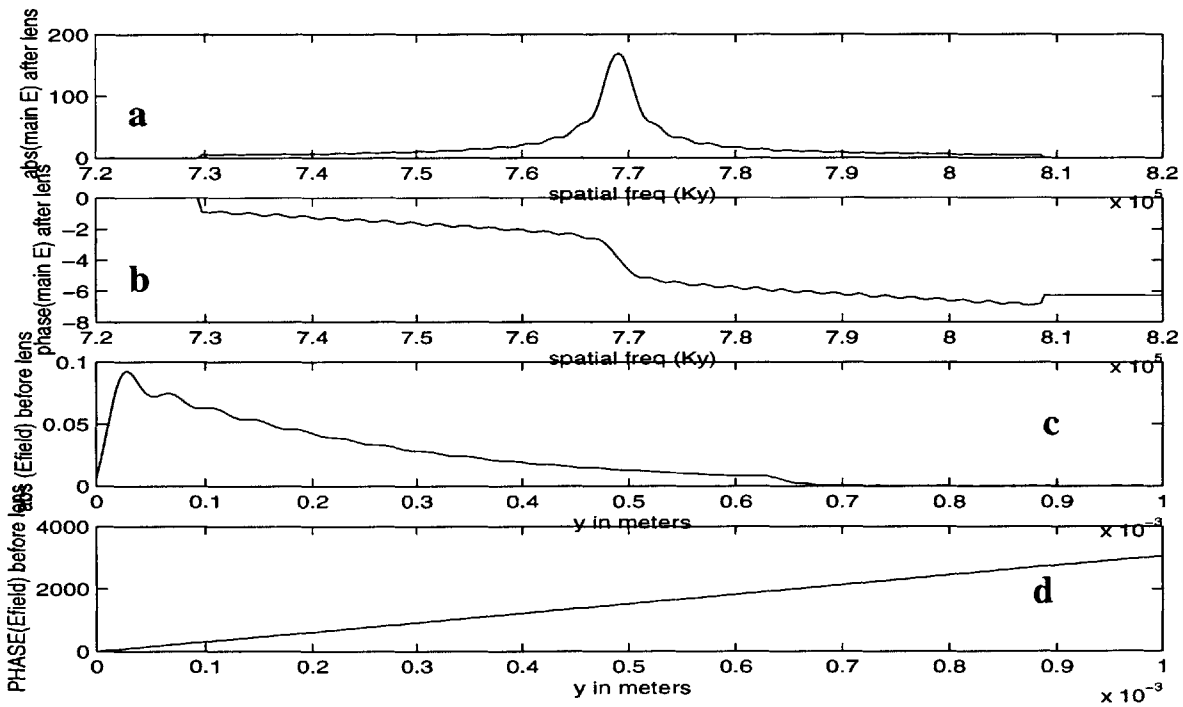


Figure 5-4 (a) magnitude profile of the Lorentzian shaped mainlobe, VU_main . (b) phase of Lorentzian mainlobe, VU_main . (c) magnitude of U_main , the IDFT of VU_main , which represents the component of the output field travelling in direction closest to incident angle. (d) phase of U_main .

Figures 5-4 a and b, respectively show the magnitude and phase profiles of the mainlobe, VU_{main} (where U denotes uniform transmissivity), of the far field pattern, VT_{total} , produced by VIPA with uniform transmissivity. VU_{main} has a Lorentzian field distribution which is evident from its symmetric magnitude profile having broad tails and a sharp peak, and its asymmetric phase profile.

By taking the inverse Fourier transform of VU_{main} , we can obtain U_{main} , the component of T_{total} travelling in the direction of the incident light, that contains most of the power. Figures 5-4 c and d, respectively show the magnitude and phase plots of U_{main} , which is the inverse Fourier transform of VU_{main} . U_{main} is much smoother than T_{total} and is clearly an exponential field with linear phase. This profile corresponds to the expected output field distribution discussed in the beginning of section 5.1.2.

5.1.3 Efficiency of VIPA with Uniform Transmissivity

Overall efficiency of the VIPA system is given by: **Efficiency = $W * M * C$** , where

W = 1 - power lost through window,

M = fraction of energy of output field in main lobe

C = coupling efficiency of main lobe to the output fiber mode.

Coupling Efficiency of VU_{main} to the output fiber depends on the distribution of the individual lobes of the far field output pattern. For the multichannel system, C also depends on the extent of overlap of adjacent lobes of different wavelengths and thus on the separation of the lobes or the angular dispersion. For simulations using an input of ten wavelengths in the range 1453.2- 1546

nm, with 0.8nm spacing; plate thicknesses near 100 μ m; and incident angle is in the range 5 -10 degrees, channel overlap was found to be negligible. Thus we consider the phase and amplitude shapes of the mainlobe of the far field output to be the main determinant of coupling efficiency. C is calculated by the method described in section 4.4.3. For this case of uniform transmissivity, the far field pattern is Lorentzian, as shown in figure 5-4 a and b. The maximum coupling efficiency attained was about 80%. Coupling efficiency did not vary significantly as plate thickness or incident angle were changed by a small amount.

M depends on the energy distribution among lobes of the output field and is highly dependent on the incident angle. Using a plate thickness of 100 μ m and a central wavelength lobe of 1550nm, an incident angle of 7.8 degrees gave M= 55%, while a smaller incident angle of 4.2 degrees improved sidelobe suppression and gave M= 87%.

The percentage of power lost at the window (1-W) is calculated as described in section 4.2 using the center wavelength of 1550nm. W depends on the wavelength, plate thickness and on the incident angle. The simulation actually takes the desired W and t as input parameters and computes the corresponding incident angle which is then used to generate the output.

Values of W, M, and C were computed for different incident angles, while the input wavelength set and plate thickness (t=100 μ m) were kept constant. An incident angle of 7.8 degrees led to an overall efficiency of 41%. Maximum overall efficiency of ~51% was achieved when the incident angle was 4.2 degrees.

5.2 VIPA with Linearly Varying Transmissivity

This section describes the results of the a VIPA simulation using a glass plate with a linear transmissivity profile along the right plate boundary. As illustrated by figure 5-2-1a, the transmission amplitude, TR is 0 from $y=0\mu\text{m}$ to the point of incidence, $y=50\mu\text{m}$, and increases linearly to 1 from $y=50\mu\text{m}$ to $y=2050\mu\text{m}$. Consequently, the reflectivity amplitude profile along this boundary is elliptic, as shown in figure 5-2-1b, using the relation in table 1 in chapter 4.

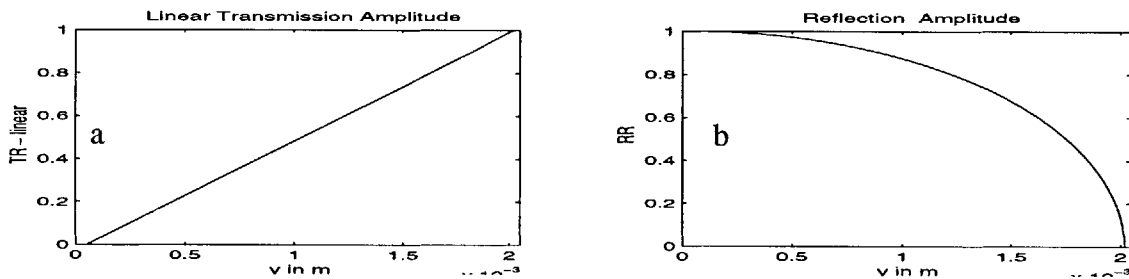


Figure 5-2-1 (a) Linear transmission amplitude along right boundary of glass plate (also y). (b) Reflection amplitude profile, along y , for linear transmissivity case.

Section 5.1.2 described how the output fields can be computed analytically for the case of uniform transmissivity. However, the same analysis can not easily be applied to this case and thus the output for the case of linear transmissivity had to be obtained using numerical analysis.

5.2.1 Output Field Profiles

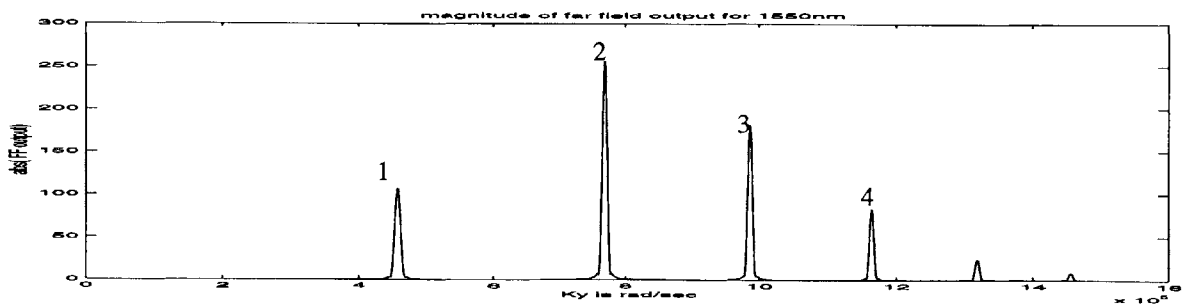


Figure 5-2-1-1 Far field output pattern using VIPA with linear transmissivity. Lobes are more symmetric than Lorentzian profiles and have linear phase. Lobes are in same position as in uniform transmissivity case.

Figure 5-2-1-1 shows the far field output pattern of a VIPA design using linear transmissivity for a single wavelength input of 1550nm. As the position of the lobes depends only on the plate thickness and wavelength, lobes of figure 5-2-1-1 are at the same position of the output lobes of the VIPA using uniform transmissivity, shown in figure 5-3. However the field distribution of the individual lobes is very different for the two VIPA designs.

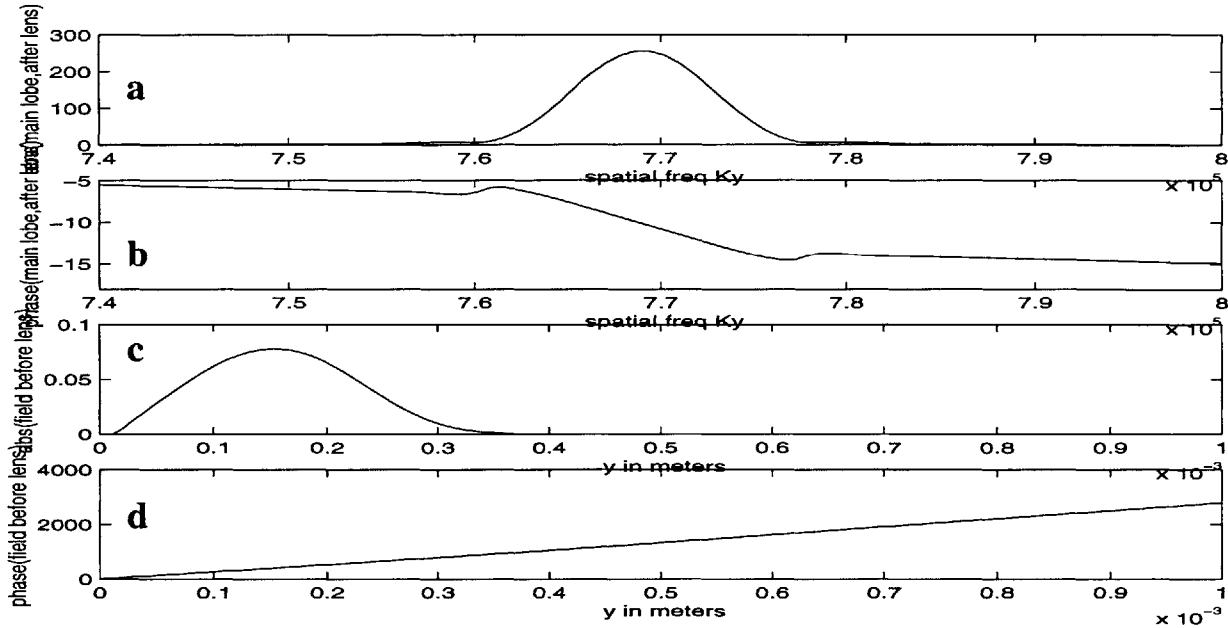


Figure 5-2-1-2 (a) magnitude of VL_main, main lobe of farfield output using linear transmissivity (b) phase of VL_main. This is approximately linear (c) magnitude of IDFT of VL_main (d) phase of IDFT of VL_main

Figure 5-2-1-2 a and b show the amplitude and phase profiles, respectively, of the main lobe, VL_main (where L denotes linear transmissivity), of the far field output of figure 5-2-1-1. Compared to the Lorentzian distribution of the uniform transmissivity VIPA output (section 5.1.2), the field distribution for the case of linear transmissivity has a wider lobe and lower tails, and more closely resembles a gaussian profile. As seen in figure 5-2-1-2b, the phase of VL_main is approximately linear, unlike the asymmetric phase profile of VU_main.

The inverse Fourier transform of VL_main gives us the relevant component of the output pattern before the lens. In the previous case, using uniform transmissivity, the output field was exponential. In this case, the output field amplitude is symmetric and bell shaped, as in figure 5-2-1-2c and the phase is as shown in figure 5-2-1-2d.

5.2.2 Efficiency of VIPA with Linear Transmissivity

The symmetric output of the VIPA with linear transmissivity leads to much higher coupling efficiencies than that of the Lorentzian output produced by a VIPA with uniform transmissivity. In this case also, C, did not vary when t and incident angle were varied by a small amount. It was possible to adjust the position and radius of the output fiber so that its gaussian mode very closely matched the symmetric amplitude profile of the output lobe. The linear phase of the output was easily corrected by placing a wedge before the collecting fiber and this increased the coupling efficiency considerably. VIPA with linear transmissivity had coupling efficiencies as high as 99%, which is a substantial improvement from the 80% coupling efficiency achieved by the uniform transmissivity system.

Values of M achieved by this system were approximately equal to those obtained by the VIPA system with uniform transmissivity. Here also, M= 55% for an incident angle of 7.8 degrees and increased to M=88% for a lower incident angle of 4.2 degrees. Power loss at the window exhibits the same variation with t, wavelength and incident angle as in the case of VIPA with uniform transmissivity. Compared to the VIPA with uniform transmissivity which had overall efficiencies of around 53%, this model achieves considerably higher coupling efficiency and thus has a higher overall efficiency of around 81%.

5.3 Far Field Output Pattern for Multi-Wavelength Input

Figure 5-3-1 shows the far field output patterns obtained for the case of two different incident angles. with an input of 10 wavelengths in the range 1553.2 nm to 1546nm, at 0.8nm spacing. In figure 5-3-1a, the incident angle is 11.5 degrees, corresponding to a window power loss of 1%, while in figure 5-3-1b, a incident angle, 8.2 degrees, leads to higher power loss of 5%, at the window. All other parameters are the same as those specified in section 5.1.1 for both figures.

These far field output patterns have many interesting features. In both cases, the envelope curve, formed by the peak values of the individual lobes, is itself a gaussian, which is expected as the input field is a gaussian. Also, the spacing between consecutive lobes decreases as ky increases and this is true for all wavelengths and incident angles

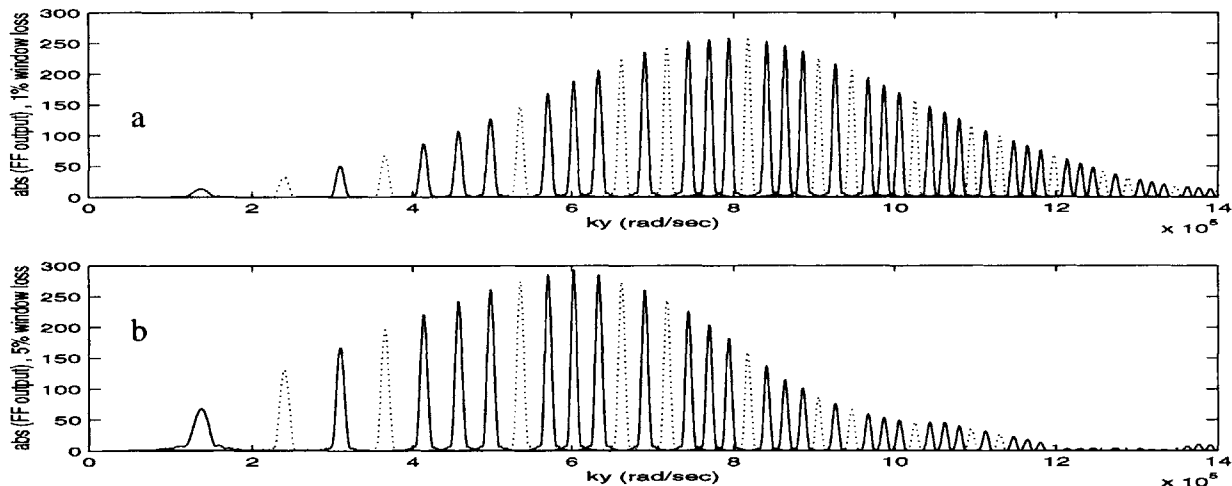


Figure 5-3-1 Far field output of ten channels for two different incident angles (a)incident angle is 11.5 degrees and $M=55\%$ (b) incident angle is 8.2 degrees and $M=88\%$. Smaller incident angle leads to better sidelobe suppression

The positions of the focused lobes in the far field pattern are determined by the wavelength and the thickness of the plate. For the two cases in figure 5-3-1, the plate thickness was kept constant at 100 μ m and the same set of wavelengths was used. Comparison of figures 5-3-1 a and b shows

that changing the angle of incidence does not affect the positions of the lobes; it only changes the distribution of energy among the lobes. As the incident angle decreases, the intensity of lobes at lower k_y increases. This change in the energy distribution also means that reducing the incident angle causes the gaussian envelope to shift to lower k_y . The fact that the lobes are spaced further apart at low k_y than at high k_y values allows the loss of energy to side lobes to be reduced by decreasing the angle of incidence.

In Figure 5-3-1a, the position of the main lobe of the central 1550 nm wavelength coincides with the envelope curve's peak. However, when the incident angle is reduced to 8.2 degrees (5% loss at window, figure 5-3-1b) the 1550nm main lobe is no longer at the center of the mainlobe; rather the lobe of the 1546.8nm output is at the center of the envelope. Section 5.4 discusses how the plate thickness can be adjusted to place the mainlobe of 1550nm output at the envelope's peak, for a particular incident angle.

5.4 Effects of Varying the Plate Thickness

The plate thickness t determines the positions of the virtual images and thus varying t can affect the focused output pattern considerably, even while other parameters such as incident angle and wavelength values remain constant. The plate thickness t , determines the spectral range of the output. The virtual images in the phased array are spaced at $2t$ along the normal to the right boundary of the plate. Reducing the plate thickness reduces the spacing of the virtual array elements. This increases the diffraction angle and thus increases the spectral efficiency of the system. A higher spectral efficiency means that the focused output can accommodate a greater range of wave-

lengths. This might allow more wavelength channels to be demultiplexed, thus increasing the capacity of the fiber optic system.

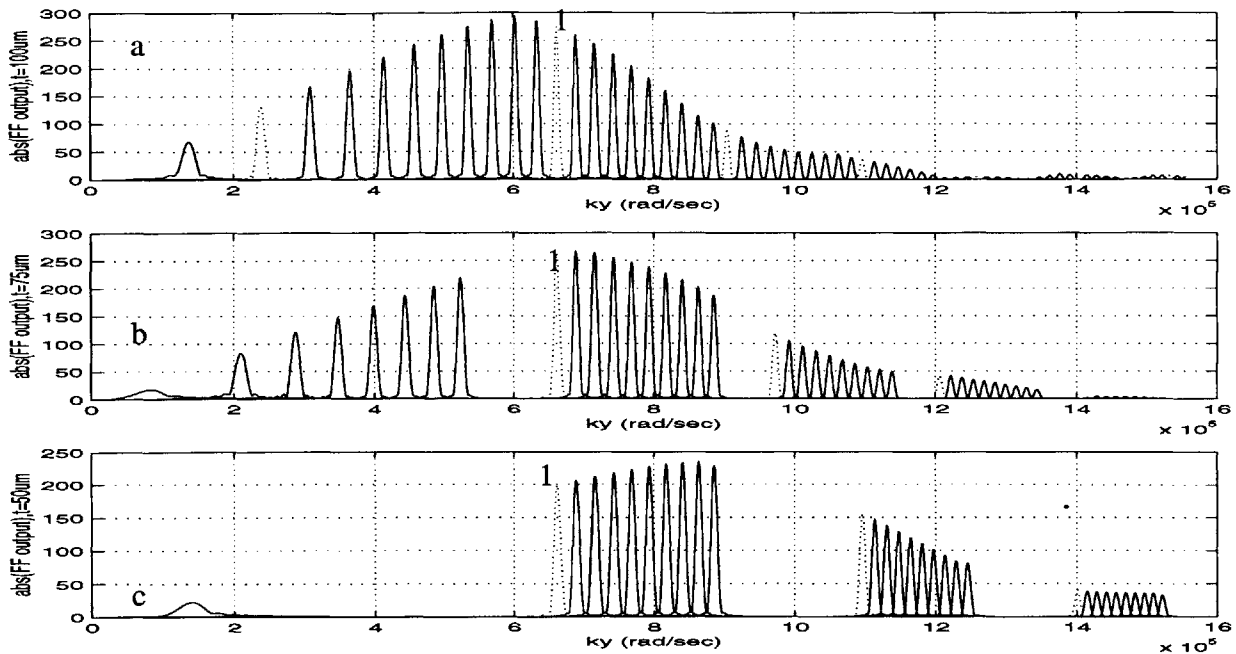


Figure 5-4-1 Far field output of ten channels for different plate thicknesses, t . (a) $t=100\ \mu\text{m}$, spectral range $\sim 8\text{nm}$ (b) $t=75\ \mu\text{m}$, spectral range $\sim 12\text{nm}$ (c) $t=50\ \mu\text{m}$, spectral range $\sim 16\text{nm}$. Reducing plate thickness increases free spectral range of VIPA system. The dotted line in each plot corresponds to the $1553.2\ \text{nm}$ lobes.

Figure 5-4-1 illustrates how reducing plate thickness increases spectral efficiency. Figure 5-4-1a is the magnitude of the far field output pattern when the plate thickness is $100\ \mu\text{m}$; 5-4-1b corresponds to a reduced plate thickness of $75\ \mu\text{m}$; and 5-4-1c corresponds to an even smaller plate thickness of $50\ \mu\text{m}$. In each case, the input consisted of 10 wavelengths within $1553.2 - 1546\ \text{nm}$ at 8nm spacing and the incident angle was 8.2 degrees. In each figure, the lobe traced by a dotted line and labelled with a '1' corresponds to a focused lobe of $1553.2\ \text{nm}$ wavelength. Spacing between two consecutive lobes of a particular wavelength gives the spectral range. Comparing the lobe positions in the three figure shows that $t=50\ \mu\text{m}$ produces the highest spectral range. The spectral range of $t=75\ \mu\text{m}$ is smaller and that of $t=100\ \mu\text{m}$ is the smallest.

Though a plate thickness of $50\mu\text{m}$ yields the highest spectral range, it also produced the greatest crosstalk between adjacent channels. Thus in most cases, the plate thickness value of about $100\mu\text{m}$ is preferred, which allows at most 10 wavelength channels at 0.8nm spacing.

Figure 5-3-1 in section 5.3 discussed how varying the incident angle shifts the envelope curve and changes the power distribution among output lobes for a fixed plate thickness of $100\mu\text{m}$. In particular, reducing the incident angle reduces the power lost to side lobes and increases power lost at the window. As the incident angle is changed, the main lobe of the 1550nm output may not always coincide with the center of the envelope, leading to suboptimal side lobe suppression. This section shows how changing the plate thickness by a very small extent can be used to place the 1550nm main lobe at the peak position of the envelope. Figure 5-4-2 examines the far field patterns for the case of three different incident angles and in each case the plate thickness, t , is adjusted so that the 1550nm main lobe is positioned at the peak of the envelope curve. Here also, the input consists of 10 wavelengths in the range 1553.2nm - 1546nm , at 0.8nm spacing. The solid line traces the output lobes of the central 1550nm wavelength while the dashed line depicts output lobes of all the other wavelengths.

Figure 5-4-2a shows the far field pattern for an incident angle of 11.5 degrees corresponding to 1% loss at the window. In this case, with a plate thickness $t=100\mu\text{m}$, the 1550 nm main lobe is at the peak position of the envelope curve and the fraction of energy in the main lobe for the 1550nm output is $M\sim 56\%$. In Figure 5-6b, the output is for a smaller incident angle of 9.4 degrees and 3% window loss. The plate thickness had to be reduced to $t=99.75\mu\text{m}$ to bring the 1550nm main lobe back to the peak position of the envelope. In this case $M\sim 75\%$. An even smaller incident angle of

8.2 degrees leads to the profile of Figure 5-6c. This high initial power loss of 5% does not distort the output fields and t is reduced to 99.7 μm to place the 1550 nm main lobe at the envelope's peak. In this case, M increases even further to $M=86\%$.

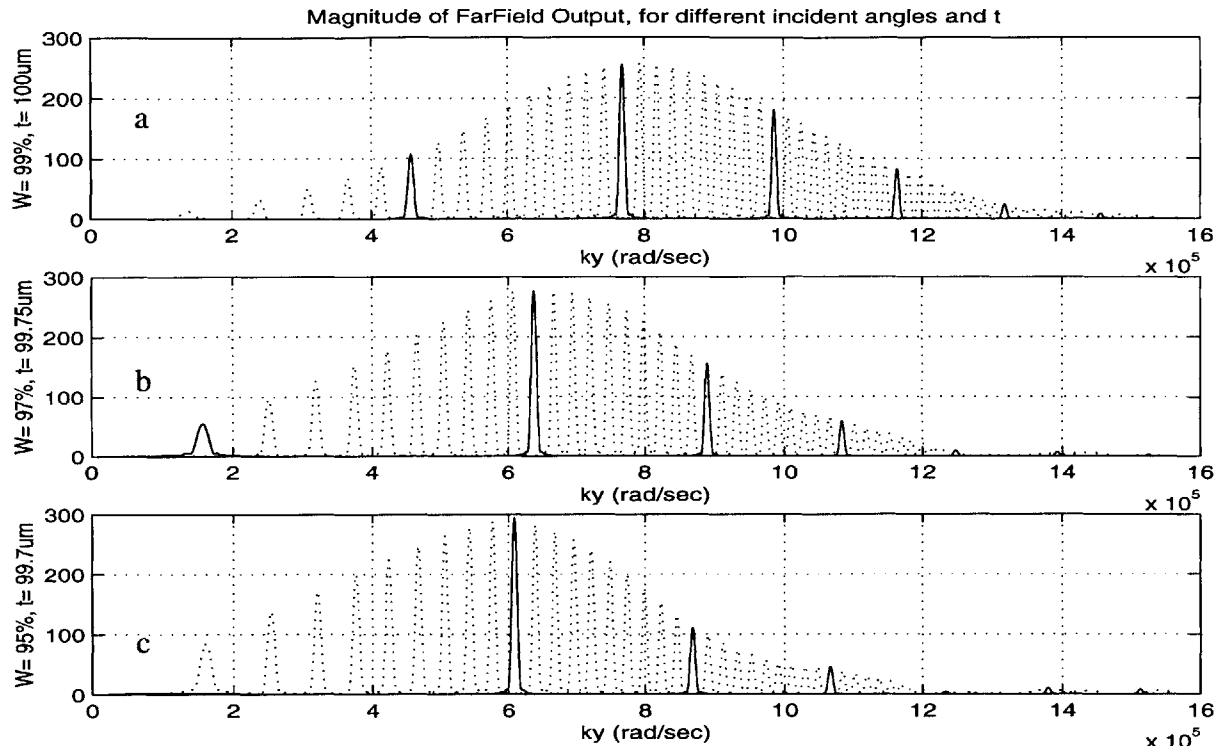


Figure 5-4-2 Adjusting t to keep 1550nm mainlobe at envelope's peak position. (a) $t= 100\mu\text{m}$ and incident angle= 11.5° (b) $t= 99.75 \mu\text{m}$ and incident angle = 9.5° (c) $t= 99.7\mu\text{m}$ and incident angle= 8.4°

Table 5-4 tabulates the parameters that correspond to the three output profiles of figure 5-4-2..

1. Table 5-4: Parameters of different incident angles and plate thicknesses

Figure with output profile	Incident Angle (degrees)	Adjusted Plate Thickness (μm)	W Power through Window	M fraction of power in mainlobe	W*M	Angular Dispersion (degree/ nm)
5_4_2 (a)	11.5	100	99%	56%	55.4%	0.008
5_4_2 (b)	9.4	99.75	97%	75%	72.8%	0.009
5_4_2 (c)	8.2	99.70	95%	86%	81.7%	0.0096

Comparison of the 1550nm lobe sizes for the three plate thickness values of figure 5-4-2 shows that reducing the incident angle shifts the energy to lobes at lower spatial frequencies, leading to

considerably better sidelobe suppression. Varying the plate thickness by a very small extent caused the lobe positions to change. Namely, reducing t caused the output lobes to shift to lower spatial frequencies. As lobe spacing is higher at lower values of k_y , reducing the plate thickness in this way has the added benefit of increasing angular dispersion. The angular dispersion for each case, measured using the 1550nm and 1548.2 nm main lobes, is listed in table 5-4. Thus we see that reducing the incident angle and the plate thickness increases the angular dispersion.

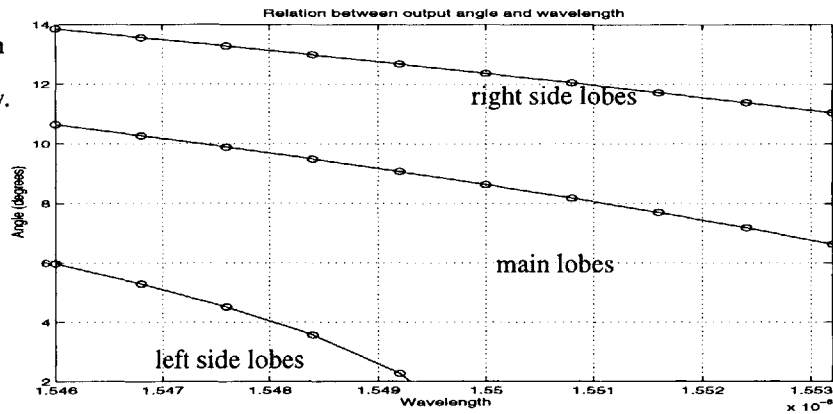
The three cases differ considerably in power efficiency. Section 5.1.3 measured efficiency as the product of W , M , and coupling efficiency C . As all three cases use the VIPA design having linear transmissivity, the coupling efficiency, C , of the lobes is approximately the same and so efficiency is directly related to $W*M$. Table 5-4 shows values of W , M and the product of W and M for the three cases. While reducing the incident angle increases window loss, it improves sidelobe suppression more than proportionately. Thus the lowest incident angle 8.2 degrees and plate thickness 99.7 μ m, has the highest $W*M$ product and thus the best power efficiency. This case also has the highest angular dispersion. Multiplying this optimized $W*M$ product with the coupling efficiency of 99% of the linear transmissivity system gives the maximum overall VIPA efficiency of 81%.

5.5 Angular Dispersion

Angular dispersion is a measure of the angular separation of adjacent, demultiplexed channels with respect to the difference in wavelength of the channels. Figure 5-5-1, shows the relation between output angle, θ_{out} , and wavelength, λ , for the VIPA demultiplexer. The output angle-wavelength relations for the two VIPA models: uniform transmissivity and linear transmissivity, were computed independently and were found to be approximately equal. The input consists of

ten wavelengths in the range 1553.2 - 1546 nm at 0.8 nm channel spacing, and 8.2 degree incident angle.

Figure 5-5-1
Plot of output angle as a function of wavelength for VIPA with uniform and linear transmissivity.



The output angle, θ_{out} , of each lobe was computed from the far-field output distribution, along k_y (spatial frequency), shown in figure 5-4-2a, and using the relation, $\theta_{out} = \sin^{-1}(k_{y_peak} / k)$, where $k = 2\pi/\lambda$, and k_{y_peak} corresponds to the peak of the lobe of λ . As seen in figure 5-4-2a, there are three sets of output lobes. The center line of figure 5-5-1 traces the $\theta_{out}-\lambda$ relation for the main lobes; the lower line is for the left (lower k_y) side lobes; and the upper line is for the right (higher k_y) side lobes. Angular dispersion is given by $|d\theta_{out} / d\lambda|$. Figure 5-5-1 shows that as λ changes, θ_{out} changes sensitively. The curve is not linear and the angular dispersion is larger at smaller θ_{out} . The angular dispersion varies from 0.36 - 1.6 degrees/nm as a function of θ_{out} , not λ .

5.6 Cross-talk from Neighboring Channels

The coupling efficiency of the 1550nm output mainlobe to a receiving fiber, fiber_1550, with optimal position and radius, is 99.35% for VIPA with linear transmissivity and is 80% for VIPA with uniform transmissivity. The crosstalk of this fiber with neighboring lobes is obtained by computing the coupling efficiency of fiber_1550 to the lobes of wavelengths near 1550nm.

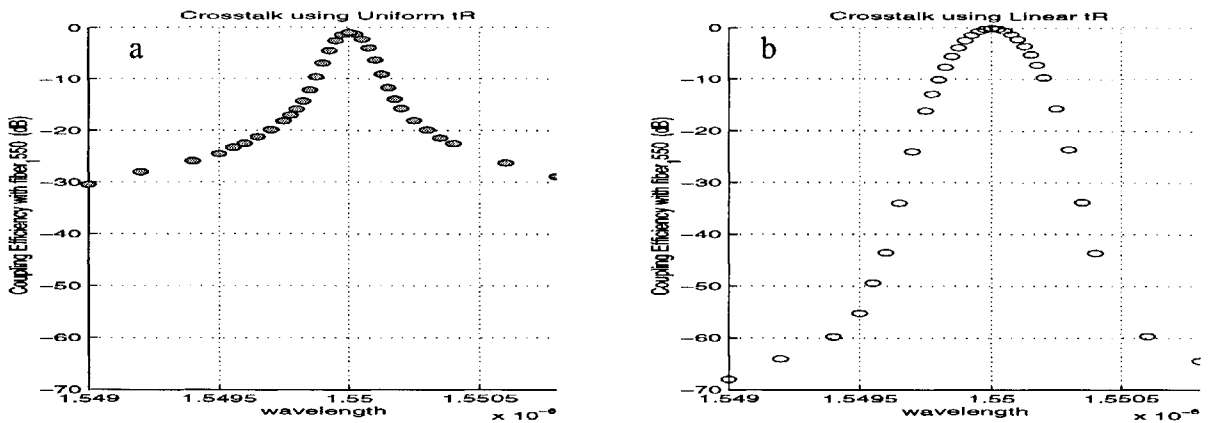


Figure 5-6-1 Crosstalk characteristic for uniform transmissivity (left) and linear transmissivity (right). Plot of coupling efficiency (dB) of receiving fiber optimized to 1550nm mainlobe to other wavelength lobes.

Figure 5-6-1 a and b show the crosstalk behavior for the uniform and linear transmissivity (tR) systems respectively. Each case plots the coupling efficiency of the gaussian mode of fiber_1550 to the mainlobes of wavelengths in the range 1549 nm- 1550.8 nm at different wavelength intervals. Within the range 1550.175nm - 1549.775nm, coupling efficiency values were obtained for smaller wavelength intervals of 0.025 nm. For the uniform transmissivity system, figure 5-6-1a shows that the crosstalk decreases rapidly for lobes within 0.2 nm of 1550nm but then decreases slowly beyond that. For the linear transmissivity system, the coupling efficiency falls slowly for lobes within 0.2 nm of 1550nm and then decreases rapidly beyond that. For channels within 0.3 nm of the 1550nm lobe, crosstalk is higher for the linear transmissivity system. For channels further than 0.3nm, cross talk is much lower for the linear tR case. Crosstalk with the neighboring channel which is 0.8nm apart is much lower for the case of linear transmissivity (~ - 65 dB) that it is for the case of uniform transmissivity (~ - 30 dB). This relative crosstalk behavior of the two systems is expected because the Lorentzian (FF-lobe using uniform tR). has a narrow peak and wide tails whereas the FF-lobe of the linear tR system has a broader peak and narrower tails.

5.7 Summary,

The simulated profiles of the field distributions inside the glass plate demonstrate that the gaussian beam progressively broadens and diminishes in magnitude and that its parabolic phase curvature increases as the beam travels through the glass plate. When the VIPA glass plate has uniform transmissivity (~5%), the output field is exponential and the far field lobes are Lorentzian. A glass plate with a linear transmissivity profile produces a more symmetric output pattern and a far field distribution that is symmetric with linear phase. The output of a linear transmissivity system has a much higher coupling efficiency (~99%) than that of the uniform transmissivity system (~80%). The linear transmissivity system also has much lower channel crosstalk than the uniform transmissivity system and thus achieves better channel isolation

The far field pattern of each channel consists of a main lobe and multiple sidelobes. Reducing the incident angle improves sidelobe suppression but worsens power loss at the window. Maximum overall efficiency of 81% is achieved by a linear transmissivity system, using the optimized beam waist and an incident angle of 8.2 degrees.

Simulation results using different glass plate thicknesses showed that reducing the plate's thickness increases the free spectral range of the system and allows more channels to be demultiplexed. In order to keep the 1550 nm main lobe at the central position of the far field envelope curve, the plate thickness must be adjusted by a very small extent ($< 1\mu\text{m}$), whenever the incident angle is changed. The angular dispersion of the uniform and linear transmissivity systems was identical and varied from 0.36 to 1.6 degrees/nm as a function of the output angle of the light, not its wavelength.

Chapter 6 Non - parallel Glass Plate

The VIPA results described so far rely on the use of a perfectly parallel glass plate of uniform thickness, $t \sim 100 \mu\text{m}$. In reality, perfectly parallel plates are difficult to construct and thus it is important to analyse the effects of plate irregularities on VIPA's performance. A common case is where the glass plate boundaries are straight but not parallel. This chapter describes the effects of using a plate with linearly varying thickness. It was found that such a plate produced considerable beam distortion which is mainly due to a quadratic phase component. Simulations showed that the distortion can be corrected by using a proper lens system.

6.1 VIPA model using a plate with linearly varying thickness

In the ideal case, the plate has uniform thickness, t_0 , and its transmissivity profile, tR , is linear with no phase ($PR=0$). In this case, the output light is collimated and the beams focus at points along the focal plane at f_0 . A plate with linearly varying thickness can be depicted as having a thickness at the top, t_{top} , which is unequal to its thickness at the bottom, t_0 . Such a plate is equivalent to a parallel plate in series with a wedge of the same material, which in turn can be represented as a parallel plate whose transmissivity profile has a linear phase component. This scheme is shown in Fig 6-1-1. The difference in thickness between the top and bottom is given by $t_{\text{dev}} = t_{\text{top}} - t_0$, and corresponds to a phase difference of $(2\pi/\lambda * 2 t_{\text{dev}})$. When $t_{\text{dev}} = \lambda/4$ ($\sim 0.4 \mu\text{m}$ for 1550nm channel), the transmissivity phase PR , increases linearly from 0 to π and when $t_{\text{dev}} = -\lambda/4$, the phase, PR , decreases linearly from 0 to $-\pi$.

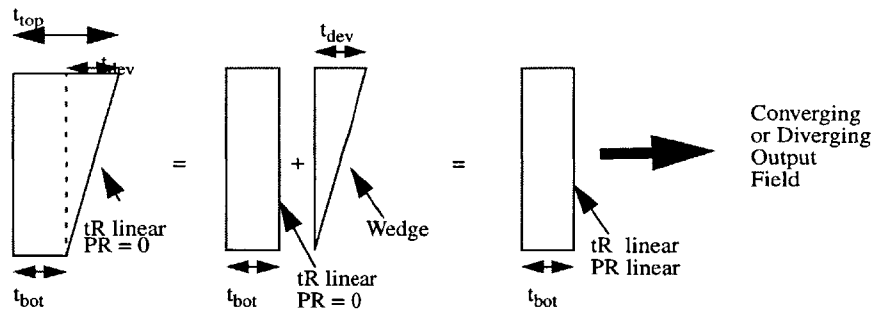


Figure 6-1-1 The VIPA glass plate with linearly varying thickness can be modelled as a glass plate with uniform thickness having transmissivity with a linear phase component.

Simulation of the plate with linear thickness is very similar to that of the parallel plate except that the transmission profile on the inner right boundary now has a linear phase component. Thus, for the plate with linear thickness, amplitude transmissivity is given by, $TR = |TR| \exp(i \cdot PR)$ and when $t_{dev} = \lambda/4$, PR increases linearly from 0 to π , along y.

Figure 6-1-2 shows the linear amplitude transmissivity, TR; the quadratically decaying reflectivity amplitude, RR; and the linear transmission phase, PR, of the plate with linear thickness.

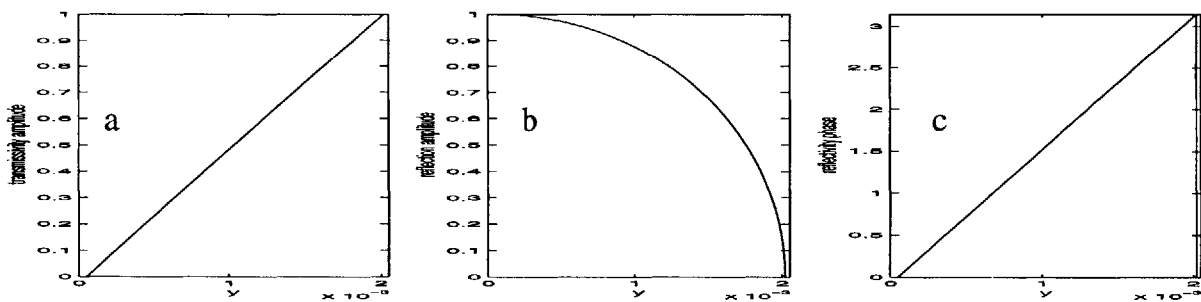


Figure 6-1-2 (a) linear amplitude transmissivity (b) amplitude reflectivity (c) linear transmission phase; used to model a glass plate with linearly varying thickness with $t_{dev} = \lambda/4$

6.2 Beam Distortion produced by plate with linearly varying thickness

The magnitude of the far-field output of the VIPA demultiplexer using a plate with linearly varying thickness and $t_{dev} = \lambda/4$ is shown in figure 6-2-1b. Figure 6-2-1a shows the ideal output using a

parallel plate. In both figures, only the mainlobes of the ten demultiplexed channels are shown.

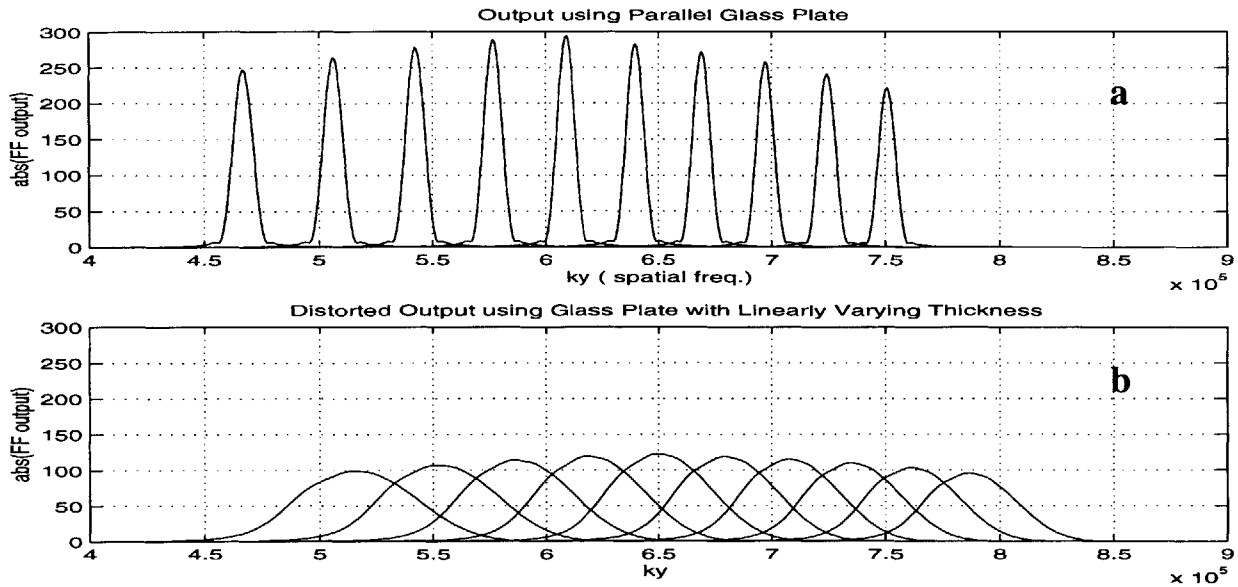


Figure 6-2-1 (a) demultiplexed output of VIPA using parallel glass plate and ten channels at 0.8 nm spacing. (b) output using plate with linearly varying thickness has much higher channel crosstalk than in (a)

After comparing the two outcomes, we see that, when the plate has non-uniform thickness, the output deteriorates considerably; the lobes become wider and overlap between lobes increases channel crosstalk drastically. Also, the lobes of 6-2-1b are shifted along ky , compared to the lobes of 6-2-1a..

To understand what causes this output distortion, we need to examine the relevant portion of the near field output for both cases. The main lobe of the far field pattern of the 1550nm wavelength's output is isolated and passed back through the lens by performing an IDFT. Let $U_{near_nonparallel}$ denote the output of the non-parallel plate and $U_{near_parallel}$ be the output of the parallel plate case, both for 1550nm channel. Figure 6-2-2a shows the magnitude profiles of $U_{near_nonparallel}$ (solid line) and $U_{near_parallel}$ (dotted line), along y , just outside the glass plate. Figure 6-2-2b shows the phase profiles of these two fields in the relevant portion of y .

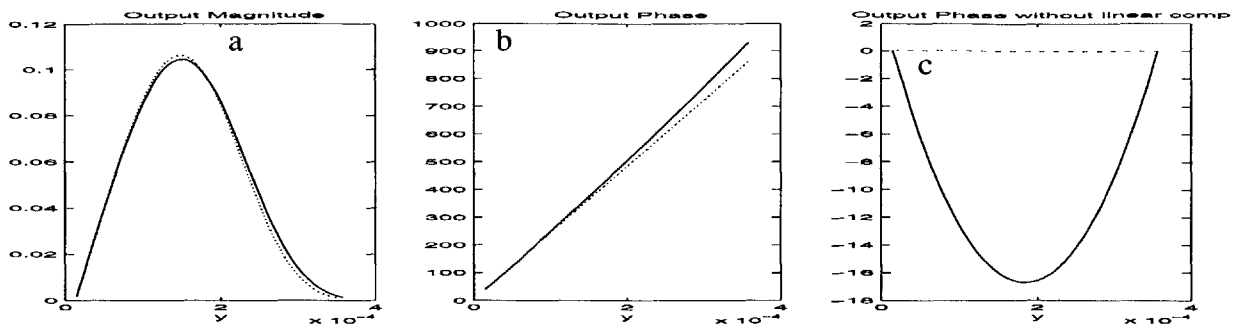
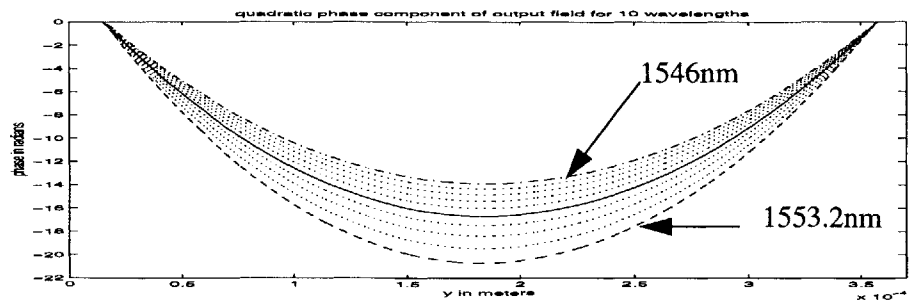


Figure 6-2-2 (a) Magnitude profile along y of Unear_nonparallel (solid) and Unear_parallel (dashed) (b) phase profile, along y , of Unear_nonparallel (solid) and Unear_parallel (dashed) (c) phase profiles of (b) with linear component subtracted shows that Unear_nonparallel has quadratic phase component.

The magnitude profiles of Unear_nonparallel and Unear_parallel are approximately equal. The phase plots show that Unear_nonparallel has a different linear phase from Unear_parallel. Now the linear phase component is removed from each of the phase profiles and the residual phase is shown in figure 6-2-2c. We see that Unear_nonparallel (solid line) has a large quadratic phase component while Unear_parallel does not. This indicates that Unear_nonparallel emerges as converging or diverging light, whereas Unear_parallel is collimated light.

A similar analysis is applied to the output beams of other wavelengths. The linear components of their phase profiles are subtracted and the residual quadratic phase is shown in figure 6-2-3. The solid curve corresponds to the quadratic phase component of the 1550nm field. The dashed line with the greatest deviation (~ 20 radians) belongs to the 1553.2 nm field; and the dash-dot line is

Figure 6-2-3 Quadratic phases of Unear_nonparallel for different wavelengths. solid line is for 1550nm; dashed line is for 1553.2 nm; dash-dot line is for 1546nm; dotted curves in between belong to the rest of the wavelengths



that of the 1546nm field. The dotted curves in between belong to the rest of the wavelength fields.

We see that using a non parallel plate introduces a linear plus a quadratic phase term, in the output field distribution, which varies with wavelength. Close inspection shows that higher order phase terms are negligible. The quadratic phase causes the output light to converge or diverge, such that the beams are focused on a plane closer to or further than f_0 , respectively. The additive linear phase alters the direction of the output light and shifts the focused beams vertically. However, the shift due to the linear phase component can be corrected easily by placing a very thin wedge before the focusing lens or by shifting the position of the receiving fibers vertically. The second order phase term produces beam profiles that come to focus slightly before or after f_0 . Thus, at f_0 , the beam profiles are much broader than beams of the parallel-plate case. The greater overlap leads to higher channel crosstalk and lower coupling efficiencies as shown in figure 6-2-1.

6.3 A Method for Correcting Beam Distortion of a Glass Plate with Linear Thickness

As the quadratic phase component introduced by the slanted plate boundary is very close to a parabola and higher order phase terms are negligible, the distorted phase can be corrected by placing a thin cylindrical lens with the appropriate focal length between the plate and focusing lens. Using a single cylindrical lens whose parabolic phase is matched to the phase component of the center wavelength, 1550nm, results in the far field output shown in figure 6-3-1b .

As shown in figure 6-2-3, the quadratic phase term is different for each wavelength. Thus using a single lens whose parabolic phase is matched to the phase distortion of the 1550nm beam restores this central beam to its ideal form while the other wavelength beams are still slightly broader than their ideal form. This is because some quadratic phase is still present in the output beams of the other wavelengths, causing them to focus just before or after the focal plane, f_0 . The error phase

term, which is the quadratic phase of figure 6-2-3 minus the lens' parabolic phase is shown in figure 6-3-1c for each wavelength lobe.

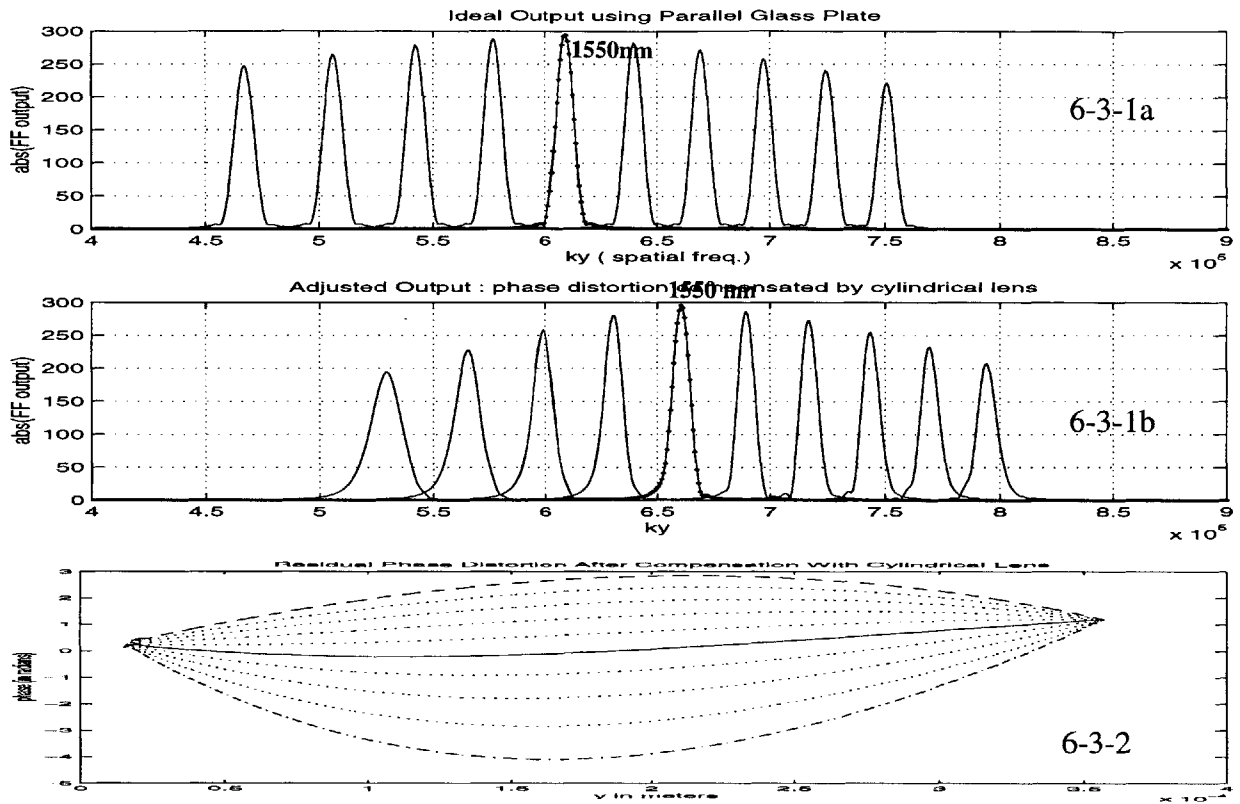


Figure 6-3-1 (a) demultiplexed output using a perfectly parallel plate (b) output with plate of linear thickness, after compensation using a thin cylindrical lens
Figure 6-3-2 Quadratic phase minus parabolic phase of cylindrical lens for different wavelengths

The focal points of the partially compensated beams are arranged on a plane that is slightly tilted with respect to the focal plane using the ideal plate. Thus to obtain all output beams at their focused points, the output fibers should be placed along this tilted plane. The outcome of such a scenario can be simulated by individually compensating the output phase distortion of each wavelength. That is, a separate parabolic phase factor is used to offset the quadratic phase of each wavelength's output. This leads to the far field output pattern shown in figure 6-3-3 b, where each wavelength lobe closely matches the parallel plate output of 6-3-3a. Such a compensation scheme leads to nearly perfect correction of the quadratic phase distortion of each wavelength. The results

presented so far in this chapter are for the case of a plate with linearly varying thickness and $t_{dev} =$

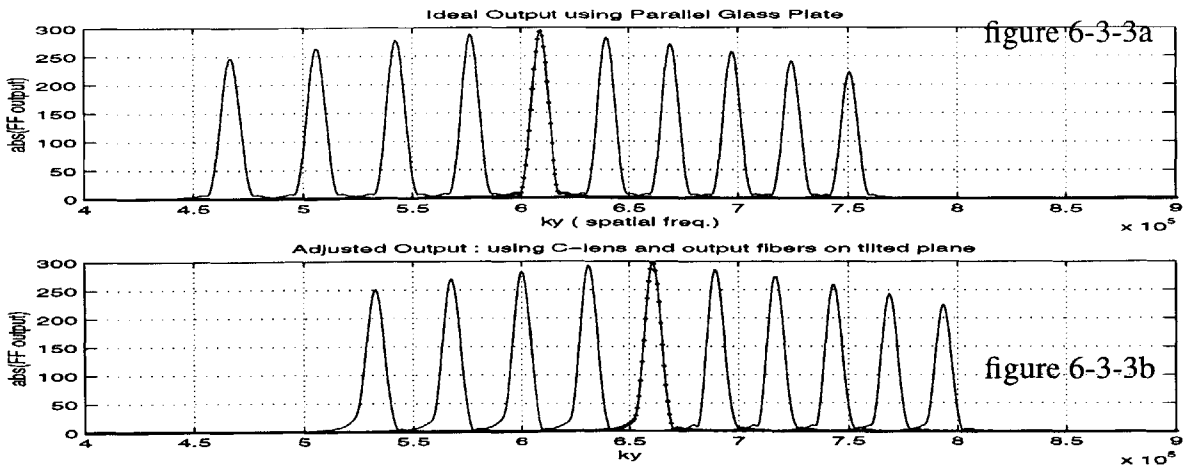
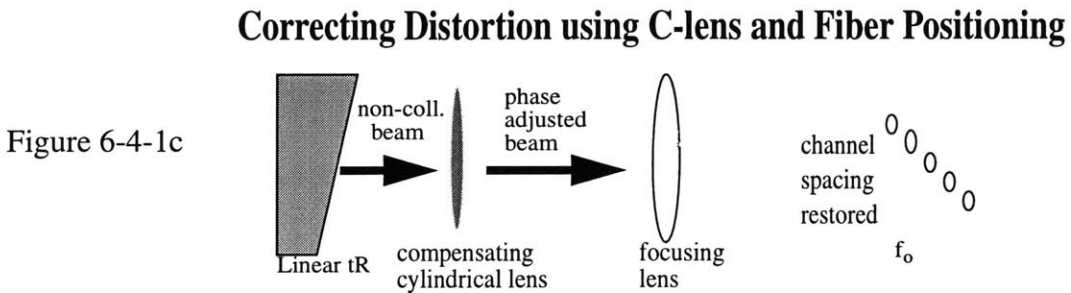
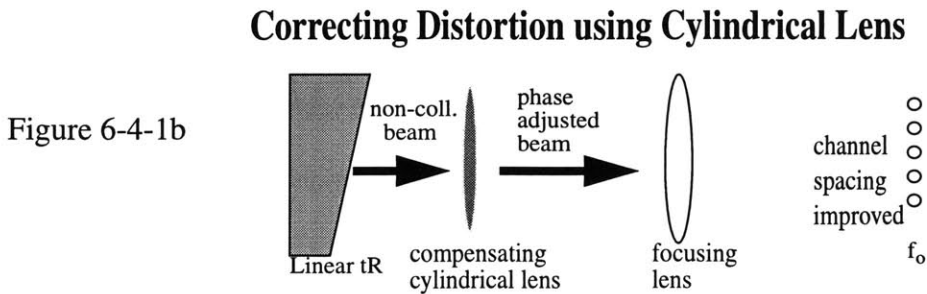
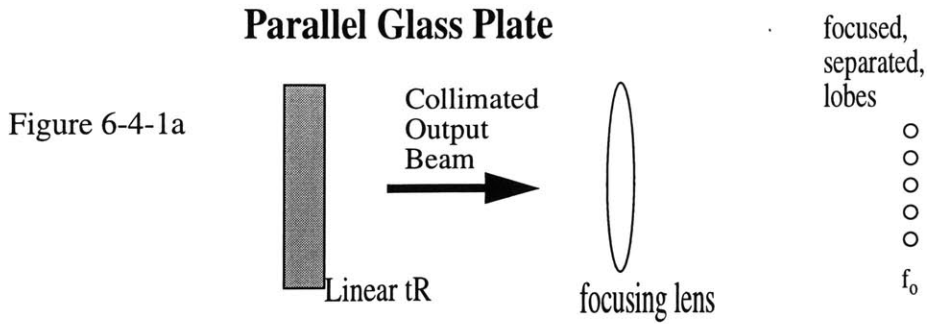


Figure 6-3-3 (a) demultiplexed output using parallel plate (b) output of plate with linear thickness using cylindrical lens and output fibers arranged on appropriately tilted plane.

$\lambda/4$. Simulations were also conducted for a glass plate with $t_{dev} = \lambda/2$, where the reflectivity phase varies linearly from 0 to 2π . This led to output fields with greater quadratic phase deviation. However, the higher order phase terms are still negligible and so the phase distortions are adequately compensated by the method discussed above.

6.4 Summary

This chapter presents a perturbation analysis for the specific case of a glass plate with linearly varying thickness. As depicted in figure 6-4-1a, the output beams after a perfectly parallel glass plate are collimated and the demultiplexed channels are well focused along the plane f_0 . When the glass plate has linearly varying thickness, the output beam is not collimated and channel crosstalk increases considerably. Numerical analysis showed that the distortion is mainly caused by a quadratic phase component and that higher order distortions are negligible.



Placing an appropriate, thin cylindrical lens after the glass plate, as shown in figure 6-4-1b, can help correct this distortion. Better compensation is achieved, by using the cylindrical lens and also arranging the output fibers along the actual tilted focal plane, as shown in figure 6-4-1c. Thus even though VIPA's performance is considerably affected by perturbations in the glass plate geometry, the resulting phase distortions can be corrected by simple optical techniques.

Chapter 7 Conclusion

This thesis presents a numerical simulation of an optical demultiplexer that uses a Virtually Imaged Phased Array. A mathematical model of the VIPA demultiplexer was developed using ray optics and fourier optics and then implemented in Matlab. Chapter 4 describes the simulation model and how it accounts for all the sources of power loss in the VIPA system.

Two main VIPA designs have been analyzed; one using a glass plate with uniform transmissivity and another using linear transmissivity. Simulation results of each design are presented and compared in chapter 5. The simulation is used to maximize efficiency by optimizing various parameters of the system such as: transmissivity coating of the glass plate, input beam waist, plate thickness, and angle of incidence.

The simulation was then used to conduct a perturbation analysis of the VIPA demultiplexing system. Chapter 6 describes the case in which a glass plate with linearly varying thickness results in high channel crosstalk. The simulation demonstrates that the distortion produced in this specific case can be corrected by a simple optical technique.

The VIPA technique can also be used as a chromatic dispersion compensator. The simulation tools developed in this project will be used and further developed by Cristopher Lin (MIT '99) to conduct a numerical analysis of the VIPA dispersion compensating system.

Bibliography

- [1] M. Shirasaki, “ Large angular dispersion by a virtually imaged phased array and its application to a wavelength demultiplexer”, Optics Letters, Vol 21, No. 5, March 1, 1996.
- [2] M. Shirasaki, “Chromatic Dispersion Compensator Using Virtually Imaged Phased Array”, IEEE Photonics Technology Letters Vol 9 No-12, December ‘97.
- [3] B. E. A. Saleh, M. C. Teich, “Fundamentals of Photonics”, Wiley Interscience publication, ‘91
- [4] H. A. Haus, “ Waves and Fields in Optoelectronics”, Prentice Hall, New Jersey, ‘84
- [5] G. P. Agrawal, “Fiber-Optic Communication Systems”, Wiley Interscience publication, ‘92
- [6] “Optical Fiber Telecommunications”, edited by I. P. Kaminow, T. L. Koch, Academic Press ‘97
- [7] This part of the code(calculation) was developed by Christopher Lin

Appendix: Simulation Code

```
% Simulation of VIPA using glass plate with Uniform Transmissivity %
% Afsana Akhter, Chris Lin, Masataka Shirasaki %
% Research Lab of Electronics . MIT%
% last updated May 18 '99 %

%%%%%%%%%%%%%%%%%%%%%%%%%%%%%%%%%%%%%%%%%%%%%%%%%%%%%%%%%%%%%%%%%%%%%%%%
GLOBAL PARAMETERS %%%%%%%%%%%%%%%%%%%%%%%%%%%%%%%%%%%%%%%%%%%%%%%%%%%%%%%%%%%%%%%%%%%%%%%%%
%%%%%%%%%%%%%%%%%%%%%%%%%%%%%%%%%%%%%%%%%%%%%%%%%%%%%%%%%%%%%%%%%%%%%%%%

n= 1.5; % refractive index of glass w.r.t air %
num_wvl = 10; % number of input wavelengths %%%%%%%%%%%%%%%%%%%%%%%%%%%%%%%%%%%%%%%%%%%%%%%%%%%%%%%%%%%%%%%%%%%%%%%%%

lamda_air(1) = 1553.2e-9;%value of input wavelengths in air%
lamda_air(2) = 1552.4e-9;
lamda_air(3) = 1551.6e-9;
lamda_air(4) = 1550.8e-9;
lamda_air(5) = 1550.0e-9;%input wavelengths centered at 1550nm %
lamda_air(6) = 1549.2e-9;
lamda_air(7) = 1548.4e-9;
lamda_air(8) = 1547.6e-9;
lamda_air(9) = 1546.8e-9;
lamda_air(10)= 1546.0e-9;

%%%%%%%%%%%%%%%%%%%%%%%%%%%%%%%%%%%%%%%%%%%%%%%%%%%%%%%%%%%%%%%%%%%%%%%% set plate thickness, window loss %%%%%%%%%%%%%%%%%%%%%%%%%%%%%%%%%%%%%%%%%%%%%%%%%%%%%%%%%%%%%%%%%%%%%%%%%
% t ~100um, adjusted slightly to place 1550nm mainlobe
% at peak position of envelope curve in far field

%t= 100e-6; % puts 1550 inmiddle for 1% loss at window, .5657 Emain/Etot%
%t = 99.75e-6;% puts 1550 inmiddle for 3% loss at window, .71 Emain/Etot%
t = 99.7e-6 % puts 1550 inmiddle for 5% loss at window, .8615 Emain/Etot%

window_loss = 5; % corresponding to t %

w_waist = sqrt(((1550e-9)/1.5) * t/pi); % optimal beam waist %
rot_theta_deg= 10; % inclination of glass slab %

for j=1:num_wvl, % compute parameters in klass%
lamda_glass(j) = lamda_air(j)/n;% wavelengths in glass %
k_glass(j) = 2*pi/lamda_glass(j);% k in glass %
zo(j) = (pi* (w_waist)^2)/ lamda_glass(j);% z= zo when W(z) = sqrt2*Wo %
end

% using powerAngle func to compute optimum i%%
theta_iglass = powerAngle(window_loss, w_waist,t)

%%%%%%%%%%%%%%%%%%%%%%%%%%%%%%%%%%%%%%%%%%%%%%%%%%%%%%%%%%%%%%%%%%%%%%%% base coordinate system %
axis_pts = 1024 * 8; % num points on axes %
ky_glass = zeros([20]); % ky in glass ( constant)%
ky_glass_vec = zeros([20,axis_pts]); % ky vector in glass %
y_base = linspace(0,2050e-6,axis_pts); % y axis % % length = 2050 microns %
```

```

rot_theta_rad= rot_theta_deg* pi/180 ; % inclination of glass slab in
radians%
y = y_base .* cos(rot_theta_rad);% y, after rotation of glass plate %
deltay = y(2) - y(1); % interval of points in y %

%%%%%%%%%%%%%%%%%%%%%%%%%%%%%%%%%%%%%%%%%%%%%%%%%%%%%%%%%%%%%%%%%%%%%%%%% determine reflectivity profiles for given window size %%%%%%%%%%%%%%%%%%%%%%%%%%%%%%%%%%%%%%%%%%%%%%%%%%%%%%%%%%%%%%%%%%%%%%%%%%

beam_posn = 50e-6; % point of inc in y, beam peak position %
RL = ones([1,axis_pts]);% reflectivity profile on left%
RR = ones([1,axis_pts]); % reflectivity profile on right%

    for ir=1:axis_pts,
        if(y(ir)< beam_posn)
            RL(ir)=0;
        else RL(ir)=1;
        end
    end

%%%%%%%%%%%%%%%%%%%%%%%%%%%%%%%%%%%%%%%%%%%%%%%%%%%%%%%%%%%%%%%%%%%%%%%%% set uniform reflectivity on right side %%%%%%%%%%%%%%%%%%%%%%%%%%%%%%%%%%%%%%%%%%%%%%%%%%%%%%%%%%%%%%%%%%%%%%%%%%
RR = sqrt(.95) * RR;
T = sqrt(1- .95);

%%%%%%%%%%%%%%%%%%%%%%%%%%%%%%%%%%%%%%%%%%%%%%%%%%%%%%%%%%%%%%%%%%%%%%%%% GENERATE GAUSSIAN BEAM %%%%%%%%%%%%%%%%%%%%%%%%%%%%%%%%%%%%%%%%%%%%%%%%%%%%%%%%%%%%%%%%%%%%%%%%%%
num_refl = 100; % number of reflections
computed%
UL = zeros([num_refl, axis_pts]); % gaussn magnitude profiles on left %
UR = zeros([num_refl, axis_pts]); % gaussn magnitude profiles on right %
%Uphase = zeros([num_refl,axis_pts]);% gaussn phase profiles %
%VL = zeros([num_refl,axis_pts]);% fft coeffson left%
%VR = zeros([num_refl,axis_pts]);% fft coeffson right%
V_indx = 1:axis_pts; % fft index - for plotting %
Uttotal = zeros([num_wvl,axis_pts]);% total field in glass plate on right%
Ttotal = zeros([num_wvl,axis_pts]); % total transmitted field,
% just outside
plate %
VTtotal = zeros([20,axis_pts]);% far field output pattern %
Z= axis_pts * 8; % for padded fft of Ttotal %%
VTtotal_extra = zeros([num_wvl, Z]); % far field output with zero padding
ky_gvec_extra = (linspace(0, 2*pi ,Z))/ deltay;
% ky vector for
zero padded case

UR_ideal = zeros([num_refl,axis_pts]);%ideal gaussian beams at input
VR_ideal = zeros([num_refl,axis_pts]);

A = 1; % amplitude of
gaussian %

for j=1:num_wvl, %%%%%%%%% constructing Ky vector %%%%%%%%%
ky_glass(j) = k_glass(j) * sin(theta_iglass * pi/180) ;
ky_glass_vec(j,:) = (linspace(0,2*pi,axis_pts))/ deltay;
Uphase = exp(i* (y -beam_posn) * ky_glass(j)); % linear pahse due to inc ang%

```

```

% -----PHASE FACTOR FOR PROPAGATION TO RIGHT-----
-----
p_fac= exp((i*(k_glass(j)*t)).*(1 - (0.5*((ky_glass_vec(j,:)/
k_glass(j)).^2))));
p_fac_left = p_fac(1,(1: axis_pts/2));
p_fac_right = ([zeros(1,axis_pts/2)]);
    for jj= 1: (axis_pts/2 ),
        p_fac_right(jj) = p_fac_left( (axis_pts/2) - (jj-1));
    end;
phase_fac = [p_fac_left p_fac_right];

% -----PHASE FACTOR FOR PROPAGATION TO LEFT-----
-----
p_fac_init= exp((i*(k_glass(j)*(-t)).*(1 - (0.5*((ky_glass_vec(j,:)/
k_glass(j)).^2))));
p_left_init = p_fac_init(1: axis_pts/2);
p_right_init = ([zeros(1,axis_pts/2)]);
    for jk= 1: (axis_pts/2 ),
        p_right_init(jk) = p_left_init( (axis_pts/2) - (jk-
1));
    end;
phase_fac_init = [p_left_init p_right_init];

% -----ideal gaussians at z=0 % -----
---
UR_ideal = A* exp(-1 *((y - beam_posn).^2)/(w_waist^2)) .* Uphase ;
U_init = ifft(fft(UR_ideal) .* phase_fac_init);% initial profiles at z= -t %
U_init_left = (1- RL) .* U_init;

UR(1,:) = ifft(fft(U_init_left) .* phase_fac); %adjusted profiles at z = 0 %
UL(1,:)= ifft((fft(RR .* UR(1,:)) .* phase_fac); %adjusted profile on left %
    for kk= 2:num_refl,
        UR(kk,:) =ifft( fft(RL .* UL(kk-1,:)).* phase_fac);
        UL(kk,:) = ifft((fft(RR .* UR(kk,:)) .* phase_fac);
    end

% -----total profile for each wavlength -----%
for ii= 1:num_refl,
    Utotal(j,:) = Utotal(j,.)+ UR(ii,.); %inner right of
plate%
    end
    Ttotal(j,:) = (-1)*T.*Utotal(j,.); % just outside of plate%
    VTtotal(j,:) = fft( Ttotal(j,.) ) ; % far field w/o padding%
    VTtotal_extra(j,:) = fft( Ttotal(j,.) , Z); % far field
withpadding%
end % done for each wavelength%
break;
%%%%%%%%%%%%%%%%%%%%%%%%%%%%%%%%%%%%%%%%%%%%%%%%%%%%%%%%%%%%%%%%%%%%%%%% isolate mainlobe of farfield VTTOTAL %%%%%%%%%

kyex = ky_gvec_extra;
yex = linspace(0,max(y_base),Z);
main = zeros([num_wvl,Z]); % matrix of mainlobes for each VTtotal_extra %

[M5,I5] = max((abs(VTtotal_extra(5,:)))); % pick peak of center wavelength %%

```

```

        % main lobes to the left of central main lobe%
[M1,I1] = max((abs(VTtotal_extra(1,1:I5)))); % to locate max of mainlobe %
[M2,I2] = max((abs(VTtotal_extra(2,1:I5))));
[M3,I3] = max((abs(VTtotal_extra(3,1:I5))));
[M4,I4] = max((abs(VTtotal_extra(4,1:I5))));
        % main lobes to the right of central main lobe %
[M6,I6] = max((abs(VTtotal_extra(6,I5:Z))));I6 = I5+I6;
[M7,I7] = max((abs(VTtotal_extra(7,I5:Z))));I7 = I5+I7;
[M8,I8] = max((abs(VTtotal_extra(8,I5:Z))));I8 = I5+I8;
[M9,I9] = max((abs(VTtotal_extra(9,I5:Z))));I9 = I5+I9;
[M10,I10] = max((abs(VTtotal_extra(10,I5:Z)))); I10 = I5+I10;

lim=300; % number of points picked from each side of peak point
        % construct field with just mainlobe, zero outside
main lobes%
main(1,(I1-lim):(I1+lim)) = VTtotal_extra(1,(I1-lim):(I1+lim));
main(2,(I2-lim):(I2+lim)) = VTtotal_extra(2,(I2-lim):(I2+lim));
main(3,(I3-lim):(I3+lim)) = VTtotal_extra(3,(I3-lim):(I3+lim));
main(4,(I4-lim):(I4+lim)) = VTtotal_extra(4,(I4-lim):(I4+lim));
main(5,(I5-lim):(I5+lim)) = VTtotal_extra(5,(I5-lim):(I5+lim));
main(6,(I6-lim):(I6+lim)) = VTtotal_extra(6,(I6-lim):(I6+lim));
main(7,(I7-lim):(I7+lim)) = VTtotal_extra(7,(I7-lim):(I7+lim));
main(8,(I8-lim):(I8+lim)) = VTtotal_extra(8,(I8-lim):(I8+lim));
main(9,(I9-lim):(I9+lim)) = VTtotal_extra(9,(I9-lim):(I9+lim));
main(10,(I10-lim):(I10+lim)) = VTtotal_extra(10,(I10-lim):(I10+lim));

%%%%%%%%%%%%%%%%%%%%%%%%%%%%%%%%%%%%%%%%%%%%%%%%%%%%%%%%%%%%%%%%%%%%%%%% calculate M, fraction of energy in Mainlobe %%%%%%%%%%%%%%%
sub = zeros([3,Z]); % select just side lobes %%
ir = 5; % just for 1550 lobe %
ratio(ir) = sum( abs(main(ir,:)).^2 ) / sum( abs(VTtotal_extra(ir,:)).^2 );
ratio(5) % energy in main lobe for 1550 nm channel %%%%%%%%%%%%%%%

%%%%%%%%%%%%%%%%%%%%%%%%%%%%%%%%%%%%%%%%%%%%%%%%%%%%%%%%%%%%%%%%%%%%%%%%%%%%%%%%%%%%%%%%%%%%%%%%%%%%%%%%%%%%%%%%%%%%%%%%%%%%%%%%%%%%%%%%%%%%%%%%
del_ky = ky_gvec_extra(2) - ky_gvec_extra(1);
norm_E = zeros([num_wvl,Z]);% for normalized main lobes%
norm_Ef = zeros([num_wvl,Z]);% for normalized fiber modes%

for in = 1: num_wvl, % NORMALIZE E field of mainlobes %%
    norm_E_fac(in) = sum((abs(main(in,:)).^2) * del_ky;
    norm_E(in,:) = main(in,:) ./ (sqrt(norm_E_fac(in)));
end

%%%%%%%%%%%%%%%%%%%%%%%%%%%%%%%%%%%%%%%%%%%%%%%%%%%%%%%%%%%%%%%%%%%%%%%% construct fiber modes %%%%%%%%%%%%%%%
ofiber = zeros([num_wvl,Z]); % for fiber mode optimized to central main lobe %
[mM1,mI1] = max((abs(main(5,:)))); % peak val and position of central mainlobe %
kyex = ky_gvec_extra; % length = 2050 microns % new ky axis pts%
yex = linspace(0,max(y_base),Z); % length = 2050 microns % new Y axis pts%
del_yex = yex(2) - yex(1);

ofw1 = (kyex(1550) - kyex(mI1))/2; % beam width of mode found by inspection%
ofiber(1,:) = mM1* exp(-1 * ((kyex - kyex(I5)).^2)/(ofw1^2)) ; %% fiber mode %

%%%%%%%%%%%%%%%%%%%%%%%%%%%%%%%%%%%%%%%%%%%%%%%%%%%%%%%%%%%%%%%%%%%%%%%% Adjust phase of fiber mode to max, coupling efficiency %%%%%%%%%
%%%%%%%%%%%%%%%%%%%%%%%%%%%%%%%%%%%%%%%%%%%%%%%%%%%%%%%%%%%%%%%%%%%%%%%%

```

```

adj_phase = zeros([num_wvl, Z]); % phase correction factor, matched to phase
                                % of main lobe %
adj_phase(1,:) = -1 * ( -4.7e-04); % computed by inspection to max coup. eff%
ofiber(1,:)= ofiber(1,:) .* exp(i* adj_phase(1,:) .* kyex); %fibermode +
phase%

for inf = 1: 10,                %% NORMALIZE fiber mode%%
    norm_fiber_fac(1) = sum((abs(ofiber(1,:)).^2) * del_ky; %%??%
    norm_Ef(1,:) = ofiber(1,:) ./ (sqrt(norm_fiber_fac(1)));
    couple_eff(inf) = abs( (sum((norm_E(inf,:)).*(norm_Ef(1,:))) *
del_ky).^2; % compute c. eff of all mainlobes to fiber mode opt for center
mainlobe%
end
couple_eff'
break;

%%%%%%%%%%%%%%%%%%%%%%%%%%%%%%%%%%%%%%%%%%%%%%%%%%%%%%%%%%%%%%%%%%%%%%%% OVERALL EFFICIENCY %%%%%%%%%
sub = zeros([3,Z]);
for ir = 1: num_wvl,
    sub(ir,:) = (abs(VTtotal_extra(ir,:)) .^2) - main(ir,:);
    ratio(ir) = sum( abs(main(ir,:)).^2 )/ sum(abs(VTtotal_extra(ir,:)).^2);
end
main_tot = [ ratio(1); ratio(2); ratio(3);]
product = (window_in/100) * main_tot' .* couple_eff % total efficiency %
%%%%%%%%%%%%%%%%%%%%%%%%%%%%%%%%%%%%%%%%%%%%%%%%%%%%%%%%%%%%%%%%%%%%%%%% end %%%%%%%%%

```

```

% Simulation of VIPA using LINEAR TRANSMISSIVITY %
% Afsana Akhter, Chris Lin, Masataka Shirasaki %
% Research Lab of Electronics . MIT%
% last updated May 18 '99 %

```

```

%%% GLOBAL PARAMETERS %

```

```

n= 1.5; % refractive index of glass w.r.t air %
num_wvl = 10;

```

```

lamda_air(1) = 1553.2e-9;%now 1550 is center wavelength %
lamda_air(2) = 1552.4e-9;
lamda_air(3) = 1551.6e-9;
lamda_air(4) = 1550.8e-9;
lamda_air(5) = 1550.0e-9;
lamda_air(6) = 1549.2e-9;
lamda_air(7) = 1548.4e-9;
lamda_air(8) = 1547.6e-9;
lamda_air(9) = 1546.8e-9;
lamda_air(10)= 1546.0e-9;

```

```

%t= 100e-6; % puts 1550 inmiddle for 1% loss at window, .5657 Emain/Etot%
%t = 99.75e-6;% puts 1550 inmiddle for 3% loss at window, .71 Emain/Etot%
t = 99.7e-6 % puts 1550 inmiddle for 5% loss at window, .8615 Emain/Etot%
window_loss = 5;
w_waist = sqrt(((1550e-9)/1.5) * t/pi);
rot_theta_deg= 10; % inclination of glass slab %

```

```

for j=1:num_wvl,
    lamda_glass(j) = lamda_air(j)/n;% wavelength in glass %
    k_glass(j) = 2*pi/lamda_glass(j);
    zo(j) = (pi* (w_waist)^2)/ lamda_glass(j);% z= zo when W(z) =
sqrt2*Wo %
end
theta_iglass = powerAngle(window_loss, w_waist,t) % using powerAngle func %%
axis_pts = 1024 * 8; % num points on axes %

```

```

ky_glass = zeros([20]);
ky_glass_vec = zeros([20,axis_pts]);
y_base = linspace(0,2050e-6,axis_pts); % y axis % % length = 2050 microns %
rot_theta_rad= rot_theta_deg* pi/180 ;
y = y_base .* cos(rot_theta_rad);
deltay = y(2) - y(1);

```

```

%%%%%%%%%%%%% determine RL and RR vector for given window size%%%%%%%%%%%%%
beam_posn = 50e-6;

```



```

RL = ones([1,axis_pts]);          % reflection coeff on left%
RR = ones([1,axis_pts]);          % reflection coeff on right%
    for ir=1:axis_pts,
        if(y(ir)< beam_posn)
            RL(ir)=0;
        else RL(ir)=1;
        end
    end

end

%%%%%%%%%%%%%%%%%%%%%%%%%%%%%%%%%%%%%%%%%%%%%%%%%%%%%%%%%%%%%%%%%%%%%%%%% LINEAR TRANSMISSIVITY %%% depends on axis_pts %%%%%%%%%
TRamp = zeros([1,axis_pts]);
TRlow = 0; TRhi = 1;
delTR = (TRhi- TRlow)/(axis_pts - 209);
for it = 1:axis_pts,
    if (y(it) <= 50.016e-6)
        TRamp(it) = 0;
    else
        TRamp(it) = delTR * (it - 209);
    end
end

end
RR = sqrt( 1 - (TRamp).^2 ) ;
T = TRamp;

%%%%%%%%%%%%%%%%%%%%%%%%%%%%%%%%%%%%%%%%%%%%%%%%%%%%%%%%%%%%%%%%%%%%%%%%% GENERATE GAUSSIAN BEAM %%%%%%%%%
num_refl = 100;
UL = zeros([num_refl, axis_pts]); % gaussn magnitude profiles on left %
UR = zeros([num_refl, axis_pts]); % gaussn magnitude profiles on right %
%Uphase = zeros([num_refl,axis_pts]);% gaussn phase profiles %
%VL = zeros([num_refl,axis_pts]);% fft coeffson left%
%VR = zeros([num_refl,axis_pts]);% fft coeffson right%
V_indx = 1:axis_pts;          % fft index - for plotting %
%phase_fac = zeros([num_refl, axis_pts]);
Uttotal = zeros([num_wvl,axis_pts]);
Ttotal = zeros([num_wvl,axis_pts]);
VTtotal = zeros([20,axis_pts]);
VTtotal_extra = zeros([num_wvl, (axis_pts * 4)]); % with zero padding
ky_gvec_extra = (linspace(0, 2*pi ,(axis_pts * 4)))/ deltay;

UR_ideal = zeros([num_refl,axis_pts]);
VR_ideal = zeros([num_refl,axis_pts]);
A = 1;          % amplitude of
gaussian %

for j=1:num_wvl,          %%%%%% constructing Ky vector %%%%%%

ky_glass(j) = k_glass(j) * sin(theta_iglass * pi/180) ;
ky_glass_vec(j,:) = (linspace(0,2*pi,axis_pts))/ deltay;

Uphase = exp(i* (y -beam_posn) * ky_glass(j)); % linear pahse due to incl%

% -----PHASE FACTOR FOR PROG TO RIGHT-----
p_fac= exp((i*(k_glass(j)*t)).*(1 -(0.5*((ky_glass_vec(j, :)/
k_glass(j)).^2))));

```

```

p_fac_left = p_fac(1,(1: axis_pts/2));
p_fac_right = ([zeros(1,axis_pts/2)]);
for jj= 1: (axis_pts/2 ),
    p_fac_right(jj) = p_fac_left( (axis_pts/2) - (jj-1));
end;
phase_fac = [p_fac_left p_fac_right];

% -----PHASE FACTOR FOR PROG TO LEFT-----

p_fac_init= exp((i*(k_glass(j)*(-t)).*(1 - (0.5*((ky_glass_vec(j,:)/
k_glass(j)).^2)))));
p_left_init = p_fac_init(1: axis_pts/2);
p_right_init = ([zeros(1,axis_pts/2)]);

for jk= 1: (axis_pts/2 ),
    p_right_init(jk) = p_left_init( (axis_pts/2) - (jk-1));
end;
phase_fac_init = [p_left_init p_right_init];

% ----- ideal gaussians at z=0 -----%

UR_ideal = A* exp(-1 *((y - beam_posn).^2)/(w_waist^2)) .* Uphase ;
U_init = ifft(fft(UR_ideal) .* phase_fac_init); %%% initial profiles at z= -t
%
U_init_left = (1- RL) .* U_init;
UR(1,:) = ifft(fft(U_init_left) .* phase_fac); %%% adjusted profiles at z = 0
%
UL(1,:)= ifft((fft(RR .* UR(1,:))) .* phase_fac);

for kk= 2:num_refl,
    UR(kk,:) =ifft( fft(RL .* UL(kk-1,:)) .* phase_fac);
    UL(kk,:) = ifft((fft(RR .* UR(kk,:))) .* phase_fac);
end

%----- total profile for each wavelength w/o zero padding%%
for ii= 1:num_refl,
    Utotal(j,:) = Utotal(j,.)+ UR(ii,.);
end
Ttotal(j,:) = (-1)*T.*Utotal(j,.);
VTtotal(j,:) = fft( Ttotal(j,.) ) ;
VTtotal_extra(j,:) = fft( Ttotal(j,:), 1024*32); %zero padding%
end
%%%%%%%%%%%%%%%%%%%%%%%%%%%%%%%%%%%%%%%%%%%%%%%%%%%%%%%%%%%%%%%%%%%%%%%%%%%%%%isolate single peak of VTTOTAL %%
Z = length(VTtotal_extra(1,:));
kyex = ky_gvec_extra;
yex = linspace(0,max(y_base),Z);
break;
%%%%%%%%%%%%%%%%%%%%%%%%%%%%%%%%%%%%%%%%%%%%%%%%%%%%%%%%%%%%%%%%%%%%%%%%%%%%%% Measure Coupling efficiency %%%
main = zeros([num_wvl,Z]); % matrix of mainlobes for each VTtotal_extra %

[M5,I5] = max((abs(VTtotal_extra(5,:))));
[M1,I1] = max((abs(VTtotal_extra(1,1:I5)))); % to locate main lobe %
[M2,I2] = max((abs(VTtotal_extra(2,1:I5))));
[M3,I3] = max((abs(VTtotal_extra(3,1:I5))));

```

```

[M4,I4] = max((abs(VTtotal_extra(4,1:I5)))); % to locate main lobe %

[M6,I6] = max((abs(VTtotal_extra(6,I5:Z))));I6 = I5+I6;
[M7,I7] = max((abs(VTtotal_extra(7,I5:Z))));I7 = I5+I7;% to locate main lobe %
[M8,I8] = max((abs(VTtotal_extra(8,I5:Z))));I8 = I5+I8;
[M9,I9] = max((abs(VTtotal_extra(9,I5:Z))));I9 = I5+I9;
[M10,I10] = max((abs(VTtotal_extra(10,I5:Z)))); I10 = I5+I10;
%----- isolate mainlobe, zero out side lobes -----%
main(1,(I1-100):(I1+100)) = VTtotal_extra(1,(I1-100):(I1+100));
main(2,(I2-100):(I2+100)) = VTtotal_extra(2,(I2-100):(I2+100));
main(3,(I3-100):(I3+100)) = VTtotal_extra(3,(I3-100):(I3+100));
main(4,(I4-100):(I4+100)) = VTtotal_extra(4,(I4-100):(I4+100));
main(5,(I5-100):(I5+100)) = VTtotal_extra(5,(I5-100):(I5+100));
main(6,(I6-100):(I6+100)) = VTtotal_extra(6,(I6-100):(I6+100));
main(7,(I7-100):(I7+100)) = VTtotal_extra(7,(I7-100):(I7+100));
main(8,(I8-100):(I8+100)) = VTtotal_extra(8,(I8-100):(I8+100));
main(9,(I9-100):(I9+100)) = VTtotal_extra(9,(I9-100):(I9+100));
main(10,(I10-100):(I10+100)) = VTtotal_extra(10,(I10-100):(I10+100));

sub = zeros([3,Z]);
ir = 5; %%%%%%%%% just for 1550 lobe %%%%%%%%%
ratio(ir) = sum( abs(main(ir,:)).^2 ) / sum( abs(VTtotal_extra(ir,:)).^2);
ratio(5) % energy in main lobe for 1550 nm channel %%%%%%%%%
del_ky = ky_gvec_extra(2) - ky_gvec_extra(1);

for in = 1: num_wvl, % NORMALIZE E field %
    norm_E_fac(in) = sum((abs(main(in,:)).^2) * del_ky;
    norm_E(in,:) = main(in,:) ./ (sqrt(norm_E_fac(in)));
end

%%%%%%%%%%%% construct fiber modes %%%%%%%%%%%%%
ofiber = zeros([num_wvl,Z]);
[mM1,mI1] = max((abs(main(5,:))));
kyex = ky_gvec_extra;
yex = linspace(0,max(y_base),Z); % length = 2050 microns% new Y axis pts%
del_yex = yex(2) - yex(1);

ofw1 = (kyex(798) - kyex(mI1))/2; % beam waists, by trial/error/inspection %
aveI5 = (kyex(I5) + kyex(I5 -1))/2;
ofiber(1,:) = mM1* exp(-1 * ((kyex - aveI5).^2)/(ofw1^2)) ; % fix these %

%%%%%%%%%%%% Adjust phases to max, coupling efficiency %%%%%%%%%
adj_phase = zeros([num_wvl, Z]);
adj_phase(1,:) = -1 * ( -5.9e-04);
ofiber(1,:)= ofiber(1,:) .* exp(i* adj_phase(1,:) .* kyex);

for inf = 1: 10, % NORMALIZE %%%
    norm_fiber_fac(1) = sum((abs(ofiber(1,:)).^2) * del_ky; %???%
    norm_Ef(1,:) = ofiber(1,:) ./ (sqrt(norm_fiber_fac(1)));
couple_eff(inf) = abs( (sum((norm_E(inf,:)).*(norm_Ef(1,:)))) * del_ky).^2
end
%%%%%%%%%%%% Loss to other modes (power in main lobe / other lobes %%
sub = zeros([3,Z]);

```

```

for ir = 1: num_wvl,
    sub(ir,:) = (abs(VTtotal_extra(ir,:)) .^2) - main(ir,:);
    ratio(ir) = sum( abs(main(ir,:)).^2 )/ sum(abs(VTtotal_extra(ir,:)).^2);
end
main_tot = [ ratio(1); ratio(2); ratio(3);]
product = (window_in/100) * main_tot' .* couple_eff % OVERALL EFFICIENCY %%

% ----- END -----%
% Simulation of VIPA using plate of LINEARLY VARYING THICKNESS %
% and LINEAR TRANSMISSIVITY %%
% Afsana Akhter, Chris LIIn, Masataka Shirasaki %
% Research Lab of Electronics . MIT%
% last updated May 18 '99 %

%%% GLOBAL PARAMETERS %

num_wvl =10; % wavelength in air %

lamda_air(1) = 1553.2e-9;%now 1550 is center wavelength %
lamda_air(2) = 1552.4e-9;
lamda_air(3) = 1551.6e-9;
lamda_air(4) = 1550.8e-9;
lamda_air(5) = 1550.0e-9;
lamda_air(6) = 1549.2e-9;
lamda_air(7) = 1548.4e-9;
lamda_air(8) = 1547.6e-9;
lamda_air(9) = 1546.8e-9;
lamda_air(10)= 1546.0e-9;

nwvl_1550 = 5; % index of center wavelength
%%%%%
n= 1.5; % refractive index of glass w.r.t air %

%t = 100e-6;% puts 1550 inmiddle for 1% loss at window, .5657 Emain/Etot%
%t = 99.75e-6;% puts 1550 inmiddle for 3% loss at window, .71 Emain/Etot%
t= 99.7e-6; % puts 1550 inmiddle for 5% loss at window, .8615 Emain/Etot%
window_loss = 5;

w_waist = sqrt(((1550e-9)/1.5) * t/pi); % depends on t %%%
rot_theta_deg= 10; % inclination of glass slab %
for j=1:num_wvl,
    lamda_glass(j) = lamda_air(j)/n;% wavelength in glass %
    k_glass(j) = 2*pi/lamda_glass(j);
    zo(j) = (pi* (w_waist)^2)/ lamda_glass(j); % z= zo when W(z) =
sqrt2*Wo %
end

theta_iglass = powerAngle(window_loss, w_waist,t) % using powerAngle func %

%%%%%%%%%%%% base coordinate system %
axis_pts = 1024 * 8; % num points on axes %

ky_glass = zeros([20]);

```

```

ky_glass_vec = zeros([20,axis_pts]);
y_base = linspace(0,2050e-6,axis_pts); % y axis % % length = 2050 microns %
rot_theta_rad= rot_theta_deg* pi/180 ;
y = y_base .* cos(rot_theta_rad);
deltay = y(2) - y(1);          %%%%% constructing Ky vector %%%%%

%%%%%%%%%%%% determine RL vector for given window size, and RR %%%%%%%%%
beam_posn = 50e-6;

RL = ones([1,axis_pts]);          % reflection coeff on left%
RR = ones([1,axis_pts]);          % reflection coeff on right%
for ir=1:axis_pts,
    if(y(ir)< beam_posn)
        RL(ir)=0;
    else RL(ir)=1;
    end
end

%%%%%%%%% LINEAR TRANSMISSIVITY %%%%%%%%% depends on axis_pts %%%%%%%%%

TRamp = zeros([1,axis_pts]);
TRlow = 0; TRhi = 1;
delTR = (TRhi- TRlow)/(axis_pts - 209);
for itt = 1:axis_pts,
    if (y(itt) <= 50.016e-6)
        TRamp(itt) = 0;
    else
        TRamp(itt) = delTR * (itt - 209);
    end
end
RR = sqrt( 1 - (TRamp).^2 ) ;

%%%%%%%%%%%% REFLECTIVITY PHASE ON RIGHT %%%%%%%%%%%%%
RRP = ones([1,axis_pts]); % phase term %
RRPlo = 0; RRPphi = pi;
delRRP = (RRPphi - RRPlo)/ (axis_pts - 209);
for ipb = 1:axis_pts,
    if (y(ipb) <= 50.016e-6)
        RRP(ipb) = 0;
    else
        RRP(ipb) = delRRP * (ipb - 209);
    end
end
RR = RR .* exp( i* RRP);
T = sqrt(1- ((abs(RR)).^2)); % T should have zero phase %

%%%%%%%%%%%%% GENERATE GAUSSIAN BEAM %%%%%%%%%%%%%
num_refl = 100;
UL = zeros([num_refl, axis_pts]); % gaussn magnitude profiles on left %
UR = zeros([num_refl, axis_pts]); % gaussn magnitude profiles on right %
%Uphase = zeros([num_refl,axis_pts]);% gaussn phase profiles %
%VL = zeros([num_refl,axis_pts]);% fft coeffson left%
%VR = zeros([num_refl,axis_pts]);% fft coeffson right%
V_indx = 1:axis_pts; % fft index - for plotting %

```

```

%phase_fac = zeros([num_refl, axis_pts]);
Uttotal = zeros([num_wvl,axis_pts]);
Ttotal = zeros([num_wvl,axis_pts]);
VTtotal = zeros([num_wvl,axis_pts]);
VTtotal_extra = zeros([num_wvl, (axis_pts * 4)]); % with zero padding
ky_gvec_extra = (linspace(0, 2*pi ,(axis_pts * 4)))/ deltay;

UR_ideal = zeros([num_refl,axis_pts]);
VR_ideal = zeros([num_refl,axis_pts]);
A = 1; % amplitude of
gaussian %

for j=1:num_wvl, %%%%%% constructing Ky vector %%%%%%
ky_glass(j) = k_glass(j) * sin(theta_iglass * pi/180) ;
ky_glass_vec(j,:) = (linspace(0,2*pi,axis_pts))/ deltay;
Uphase = exp(i* (y -beam_posn) * ky_glass(j)); % linear pahse due to incl%

% -----PHASE FACTOR FOR PROG TO RIGHT-----
p_fac= exp((i*(k_glass(j)*t)).*(1 -(0.5*((ky_glass_vec(j, :)/
k_glass(j)).^2))));
p_fac_left = p_fac(1,(1: axis_pts/2));
p_fac_right = ([zeros(1,axis_pts/2)]);
for jj= 1: (axis_pts/2 ),
p_fac_right(jj) = p_fac_left( (axis_pts/2) - (jj-1));
end;
phase_fac = [p_fac_left p_fac_right];

% -----PHASE FACTOR FOR PROG TO LEFT-----

p_fac_init= exp((i*(k_glass(j)*(-t)).*(1 -(0.5*((ky_glass_vec(j, :)/
k_glass(j)).^2))));
p_left_init = p_fac_init(1: axis_pts/2);
p_right_init = ([zeros(1,axis_pts/2)]);

for jk= 1: (axis_pts/2 ),
p_right_init(jk) = p_left_init( (axis_pts/2) - (jk-1));
end;
phase_fac_init = [p_left_init p_right_init];

% -----ideal gaussians at z=0 -----%
UR_ideal = A* exp(-1 *((y - beam_posn).^2)/(w_waist^2)) .* Uphase ;
U_init = ifft(fft(UR_ideal) .* phase_fac_init); % initial profiles at z= -t %
U_init_left = (1- RL) .* U_init;
UR(1,:) = ifft(fft(U_init_left) .* phase_fac); % adjusted profiles at z = 0 %
UL(1,)= ifft((fft(RR .* UR(1,:))) .* phase_fac);

for kk= 2:num_refl,
UR(kk,:) =ifft( fft(RL .* UL(kk-1,:)).* phase_fac);
UL(kk,:) = ifft((fft(RR .* UR(kk,:))) .* phase_fac);
end

% ----- total profile for each wvlength w/o zero padding%
for ii= 1:num_refl,
Uttotal(j,:) = Uttotal(j, :)+ UR(ii, :);

```

```

end
Ttotal(j,:) = (-1)*T.*Utotal(j,:);
%VTtotal(j,:) = fft( Ttotal(j,:)) ;
VTtotal_extra(j,:) = fft( Ttotal(j,:), 1024*32); %zero padding%
end

% ----- isolate single peak of VTTOTAL----- %%
Z = length(VTtotal_extra(1,:));

M= zeros([1,num_wvl]); % pick main and project back through lens %
I= zeros([1,num_wvl]);
VTtotal_solo = zeros([num_wvl,Z]);
Utotal_mod = zeros([num_wvl,Z]);
VTtotal_mod = zeros([num_wvl,Z]);
Ut_mod_phase= zeros([num_wvl,Z]);

% -----pick lobes from VTTtotal_extra -----

[M(nwvl_1550) I(nwvl_1550)] = max( abs(VTtotal_extra(nwvl_1550,:)));
%%%%%%%%%%%% for lobes right of 1550 lobe %
for imm= (nwvl_1550 + 1):num_wvl, % set range to pick mainlobes from %%%%
[M(imm) I(imm)]
=max(abs(VTtotal_extra(imm,I(nwvl_1550):(I(nwvl_1550)+1600)))));
I(imm) = I(nwvl_1550)+ I(imm);
end;
%%%%%%%%%%%% for lobes left of 1550 lobe %
for iml= 1:(nwvl_1550 - 1), % set range to pick mainlobes from %%%%
min_indx= 600;
[M(iml) I(iml)] =max(abs(VTtotal_extra(iml,(I(nwvl_1550) -
min_indx):I(nwvl_1550)))));
I(iml) = (I(nwvl_1550) - min_indx)+ I(iml);
end;
% -----

for im=1:num_wvl,
VTtotal_solo(im,:) = [zeros([1,(I(im)-201)]) VTtotal_extra(im,(I(im)-200) :
(I(im)+200)) zeros([1, Z-(I(im)+200)]) ];
Utotal_mod(im,:) = ifft(VTtotal_solo(im,:));
%VTtotal_mod(im,:) = fft(Utotal_mod(im,:));
Ut_mod_phase(im,:)= phase(Utotal_mod(im,:));
end;

%%%%%%%%%%%%%%%%%%%%%%%%%%%%%%%%%%%%%%%%%%%%%%%%%%%%%%%%%%%%%%%%%%%%%%%%Measure Coupling efficiency || NOT DONE || %%%
del_ky = ky_gvec_extra(2) - ky_gvec_extra(1);
% deleted portions here %
%%%%%%%%%%%%%%%%%%%%%%%%%%%%%%%%%%%%%%%%%%%%%%%%%%%%%%%%%%%%%%%%%%%%%%%% construct fiber modes %%%%%%%%%
%%% use Ky space %%%%
% deleted a bunch
kyex = ky_gvec_extra;
yex = linspace(0,max(y_base),Z); % length = 2050 microns% new Y axis pts%
del_yex = yex(2) - yex(1);

%***** remove phase distortion*****%

```

```

plo= 240;      % select index of relevant region %
plen = 5710; % same plo plen for 1550, 1549, 1548 %
kk= plo:plen;      % for part of phase curve of interest %

% linear segment for region plo:plen only %
test = zeros([num_wvl, (plen - plo+1)]);
parab_ph = zeros([num_wvl, (plen - plo+1)]);
pphase_wh = zeros([num_wvl, Z]);
pmin = zeros([1,num_wvl]);
pj = zeros([1,num_wvl]);
%par_ph_sh = zeros([num_wvl,(((plen - plo)/2)+1)]);    %% fix%%%%%

for it=1:num_wvl,
test(it,:)=linspace(Ut_mod_phase(it,plo),Ut_mod_phase(it,plen),(plen -
plo+1));
parab_ph(it,:) = Ut_mod_phase(it,plo:plen) - test(it,:);
pphase_wh(it,:) = [zeros([1,(plo-1)]) parab_ph(it,:) zeros([1,(Z - plen)])];
[pmin(it) pj(it)] = min(parab_ph(it,:));
par_ph_sh = parab_ph(1,(pj(1):length(parab_ph(1,:)))) - pmin(1);
end;

%-----construct comp parab, separately for each wvl% -----%

%actph_right = zeros([num_wvl,length(tparab)]);
%estph_right = zeros([num_wvl,length(tparab)]);
PL = length(par_ph_sh);
actph_right = zeros([num_wvl,length(par_ph_sh)]);
estph_right = zeros([num_wvl,length(par_ph_sh)]);
%estph_left = zeros([num_wvl,((plen - plo)/2)]);
%estph_whole = zeros([num_wvl,length(tparabwhole)]);
estph_left = zeros([num_wvl, (length(estph_right) -1 )]);
%estph_whole = zeros([num_wvl,]);
estph_whole = zeros([num_wvl, length(estph_right)+ length(estph_left)]);
phfor_comp = zeros([num_wvl,Z]);
yp = yex(1:length(par_ph_sh));

for iy=1:num_wvl,    %% equiv tp par_ph_sh %%%%%%%%%%%
actph_right(iy,:) = parab_ph(iy,(pj(1):length(parab_ph(1,:)))) - pmin(iy);
end

estph_right(1,:) = ((26400*yp).^2);
estph_right(2,:) = ((25800*yp).^2);
estph_right(3,:) = ((24900*yp).^2);
estph_right(4,:) = ((24400*yp).^2);
estph_right(5,:) = ((23700*yp).^2); %% use to be 21500 %%%%%%%%%
estph_right(6,:) = ((23700*yp).^2);
estph_right(7,:) = ((23200*yp).^2);
estph_right(8,:) = ((22700*yp).^2);
estph_right(9,:) = ((22200*yp).^2);
estph_right(10,:)= ((21700*yp).^2);

for iyl= 1:num_wvl,
    for iyi= 1:(PL-1),

```



```

        estph_left(iyl,iyi) = estph_right(iyl,(PL- (iyi -1)));
    end
estph_whole(iyl,:) = [estph_left(iyl,:) estph_right(iyl,:)] + pmin(iyl);
phfor_comp(iyl,:) = [zeros([1,(plo -1)]) estph_whole(iyl,:) zeros([1,(Z -
(2*PL -1 + plo -1))])];
end
% ----- compensate actual phases with estimated phases, indiv wvl %%%
act_minus_est = zeros([num_wvl,Z]);
restore_lin = zeros([num_wvl,Z]);
Ut_adj_each=zeros([num_wvl,Z]);
Vt_adj_each=zeros([num_wvl,Z]);

for iqi=1:num_wvl,
        % indiv adj %%%
act_minus_est(iqi,:) = pphase_wh(iqi,:) - phfor_comp(iqi,:); % indiv adj %%%
        %% common adj %%
%act_minus_est(iqi,:) = pphase_wh(iqi,:) - phfor_comp(5,:); %% common adj %%

restore_lin(iqi,:) = [Ut_mod_phase(iqi,1:(plo-1)) test(iqi,:)]
Ut_mod_phase(iqi,(plen+1):Z)];
Ut_adj_each(iqi,:) =abs(Utotal_mod(iqi,:)) .* exp(i*act_minus_est(iqi,:))
.*exp(i*restore_lin(iqi,:));
Vt_adj_each(iqi,:) = fft(Ut_adj_each(iqi,:));

end;
%break;

% ----- %%%

figure(10); d1 = 6; d2= 7; d3 = 8; d4 = 9; d5= 10;

subplot(5,2,1),plot(parab_ph(d1,:), 'c');
        hold on;plot(estph_whole(d1,:), 'y'); hold off;
subplot(5,2,2),plot(act_minus_est(d1,plo:plen), 'c');
diffd1 = max(act_minus_est(d1,:)) - min(act_minus_est(d1,:))

subplot(5,2,3),plot(parab_ph(d2,:), 'm');
        hold on;plot(estph_whole(d2,:), 'y'); hold off;
subplot(5,2,4),plot(act_minus_est(d2,plo:plen), 'm');
diffd2 = max(act_minus_est(d2,:)) - min(act_minus_est(d2,:))

subplot(5,2,5),plot(parab_ph(d3,:), 'r');
        hold on;plot(estph_whole(d3,:), 'y'); hold off;
subplot(5,2,6),plot(act_minus_est(d3,plo:plen), 'r');
diffd3 = max(act_minus_est(d3,:)) - min(act_minus_est(d3,:))

subplot(5,2,7),plot(parab_ph(d4,:), 'g');
        hold on;plot(estph_whole(d4,:), 'y'); hold off;
subplot(5,2,8),plot(act_minus_est(d4,plo:plen), 'g');
diffd4 = max(act_minus_est(d4,:)) - min(act_minus_est(d4,:))

subplot(5,2,9),plot(parab_ph(d5,:), 'w');
        hold on;plot(estph_whole(d5,:), 'y'); hold off;
subplot(5,2,10),plot(act_minus_est(d5,plo:plen), 'w');

```

```

diffd5 = max(act_minus_est(d5,:)) - min(act_minus_est(d5,:))
break;

%% ----- end -----

%%%%%%%%%%%%%%%%%%%%%%%%%%%%%%%%%%%%%%%%%%%%%%%%%%%%%%%%%%%%%%%%%%%%%%%% function uedsed in other programs to compute optimum incident angle%
%%%%%%%%%%%%%%%%%%%%%%%%%%%%%%%%%%%%%%%%%%%%%%%%%%%%%%%%%%%%%%%%%%%%%%%% in glass, given plate thickness and desired powerloss at window.%

% Afsana Akhter, Chris Lin, M. Shirasaki
% Rsearch Lab of Electronics, MIT
% last Updated on May 18 '99

function theta = powerAngle(powerLoss, w_waist,t)

powerLoss = powerLoss/100;%powerLoss in percent

                                %beam waist at input of plate
waist = w_waist;%beam waist at point of inc %%
zo = (pi* (waist)^2)/ (1550e-9 / 1.5);
w_window = waist * sqrt( 1 + (2*t/zo)^2 );%beam waist at window %

                                %waist of power profile
powerWaist = w_window/sqrt(2);

                                %distance between power profile center and reflectivity change
offset = erfinv(1-powerLoss*2)*powerWaist*sqrt(2);
thetainair= atan(offset/t)*180/pi;
theta= thetainair / 1.55;

```

701-14